Dalton Transactions

Accepted Manuscript

ROYAL SOCIETY OF CHEMISTRY

www.rsc.org/dalton

Synthesis, Characterization, Thermal Properties and Antiproliferative Potential of Copper(II) 4′-phenyl-terpyridine Compounds

Zhen Ma,[a,b] * Bian Zhang,[a] M. Fátima C. Guedes da Silva,[b] * Joana Silva,[c] Ana Soraia Mendo,[c] Pedro Viana Baptista,[c] Alexandra R. Fernandes,[b,c] * Armando J.L. Pombeiro [b]

[a] Guangxi Key Laboratory of Petrochemical Resource Processing and Process Intensification Technology, School of Chemistry and Chemical Engineering, Guangxi University, Nanning 530004, P. R. China, mzmzfll0090@sina.com

[b] Centro de Química Estrutural, Complexo I, Instituto Superior Técnico, Universidade de Lisboa, Av. Rovisco Pais, 1049-001, Lisboa, Portugal, E-mail: fatima.guedes@tecnico.ulisboa.pt

[c] UCIBIO, Departamento de Ciências da Vida, Faculdade de Ciências e Tecnologia, Universidade Nova de Lisboa, Caparica, Portugal, E-mail: ma.fernandes@fct.unl.pt

Abstract

Reactions between 4'-phenyl-terpyridine (L) and several Cu(II) salts (*p*-toluenesulfonate, benzoate and *o*-, *m*- or *p*-hydroxybenzoate) led to the formation of $[Cu(p\text{-}SO_3C_6H_4CH_3)L(H_2O)_2](p\text{-}SO_3C_6H_4CH_3)$ (**1**), $[Cu(OCOPh)_2L]$ (**2**), $[Cu(o\text{-}OCOC_6H_4OH)_2L]$ (**3**), $[Cu(m\text{-}OCOC_6H_4OH)_2L]\cdot MeOH$ (**4**·MeOH) and $[Cu(p\text{-}OCOC_6H_4OH)_2L]\cdot 2H_2O$ (**5**·2H$_2$O), which were characterized by elemental and TG-DTA analyses, ESI-MS, IR spectroscopy and single crystal X-ray diffraction, as well as by conductivimetry. In all structures the Cu atoms present N_3O_3 octahedral coordination geometries which, in **2** – **5**, are highly distorted as a result of the chelating-bidentate mode of one of the carboxylate ligands. Intermolecular π···π stacking interactions could also be found in **2** – **5** (in the 3.569 – 3.651 Å range and involving solely the pryridyl rings). Medium-strong hydrogen bond interactions lead to infinite 1D chains (in **1** and **4**) and to an infinite 2D network (in **5**).

Compounds **1** and **4** show high *in vitro* cytotoxicity towards HCT116 colorectal carcinoma and HepG2 hepatocellular carcinoma cell lines. The antiproliferative potential of compound **1** is due to an increase of the apoptotic process that was confirmed by Hoechst staining, flow cytometry and RT-qPCR. All compounds are able to non-covalently intercalate the DNA helix and to induce *in vitro* pDNA double-strand breaks in the absence of H_2O_2. Concerning compound **1**, the hydroxyl radical and singlet oxygen do not appear to be involved in the pDNA cleavage process and the fact that this cleavage also occurs in the absence of molecular oxygen points towards a hydrolytic mechanism of cleavage.

Introduction

Metal terpyridine compounds attract great attention and their synthesis is a topic of major current interest with implications in the fields of catalysis, photoluminescence, materials science and pharmacology because they show interesting properties in such fields.[1-12] Indeed, terpyridines have been extensively studied due to their ability to form a wide range of metal complexes that can efficiently intercalate in nucleic acid molecules, and therefore presenting themselves as promising antitumour agents.[13-14] Functionalized terpyridines have been used in antitumour research and tested in several clinical applications as DNA binding agents[15-16]. Terpyridine compounds often present a strong cytotoxicity against several human cancer cell lines, and structure–activity relationship studies indicate that the [2,2';6',2"]-terpyridine skeleton displays a significant role in this cytotoxicity[14, 17].

Since the discovery and clinical approval of cisplatin, efforts have been made to develop novel antitumour drugs that can overcome its systemic and organ-specific toxicities and to improve chemotherapy clinical effectiveness[18, 19]. Among the non-platinum compounds with antitumour potential, transition-metal complexes, *e.g.* with copper, have been investigated on the assumption that endogenous metals may be less toxic[18]. As shown by others[20, 21], several terpyridine copper(II) complexes present very promising cytotoxicity against several tumour cell lines, including

cervical carcinoma cells (HeLa), breast cancer cells (MCF-7), hepatocellular carcinoma cells (HepG2) and human lung carcinoma cells (H1299).

The antitumour activities of terpyridine compounds should depend not only on the terpyridine ligands and metal ion, but also on the co-ligands. Hence, in order to explore such a dependence, we synthesized a series of new copper complexes of a multi-pyridyl ligand (4′-phenyl-terpyridine) bearing benzoate ($PhCOO^-$), *o*-, *m*- or *p*-hydroxyl substituted benzoate or *p*-tolylsulfonate (p-$CH_3PhSO_3^-$) as anionic ligands. They were characterized by elemental analysis, IR, X-ray structural analysis, and their thermal properties and biological properties were studied.

2. Results and discussion

2.1. Syntheses and characterization of the complexes

The Cu(II) complexes [Cu(p-$SO_3C_6H_4CH_3$)L(H_2O)$_2$](p-$SO_3C_6H_4CH_3$) (**1**), [Cu(OCOPh)$_2$L] (**2**), [Cu(o-$OCOC_6H_4OH$)$_2$L] (**3**), [Cu(m-$OCOC_6H_4OH$)$_2$L] (**4**) and [Cu(p-$OCOC_6H_4OH$)$_2$L] (**5**) were synthesized (Scheme 1) by reaction of L with the appropriate Cu(II) salt added in stoichiometric amounts, i.e. Cu(p-SO_3PhCH_3)$_2$·MeOH, Cu(OCOPh)$_2$·MeOH, Cu(o-$OCOC_6H_4OH$)$_2$·2H_2O, Cu(m-$OCOC_6H_4OH$)$_2$·0.5H_2O or Cu(p-$OCOC_6H_4OH$)$_2$·H_2O, respectively, usually in a methanol, methanol:CH_2Cl_2 or methanol:CH_2Cl_2:DMF solution. The reactions usually proceeded smoothly at room temperature and the complexes were isolated after 24 h, in good to high yields (45 – 85 %).

The five complexes were isolated as blue (**1**, **2**) or green (**3** – **5**) solids, which were characterized (see experimental) by elemental analysis, IR spectroscopy, single-crystal X-ray diffraction, ESI-MS and TG-DTA analyses, and also by conductivimetry. Suitable crystals for X-ray diffraction analysis were obtained upon crystallization from slow evaporation of a methanol solution (**1**, **2** and **4**), from the mother liquor solution (**3**), or from the mother liquor solution by slow diffusion of diethyl ether (**5**).

The electronic absorption spectra of compounds **1 - 5** in 5mM Tris-HCl and 50 mM NaCl buffer (pH 7.2) are similar in shape and exhibit an intense absorption band in the UV region (287 nm for compounds **1**,**2**, **4** and **5**; 295 nm for compound **3**).

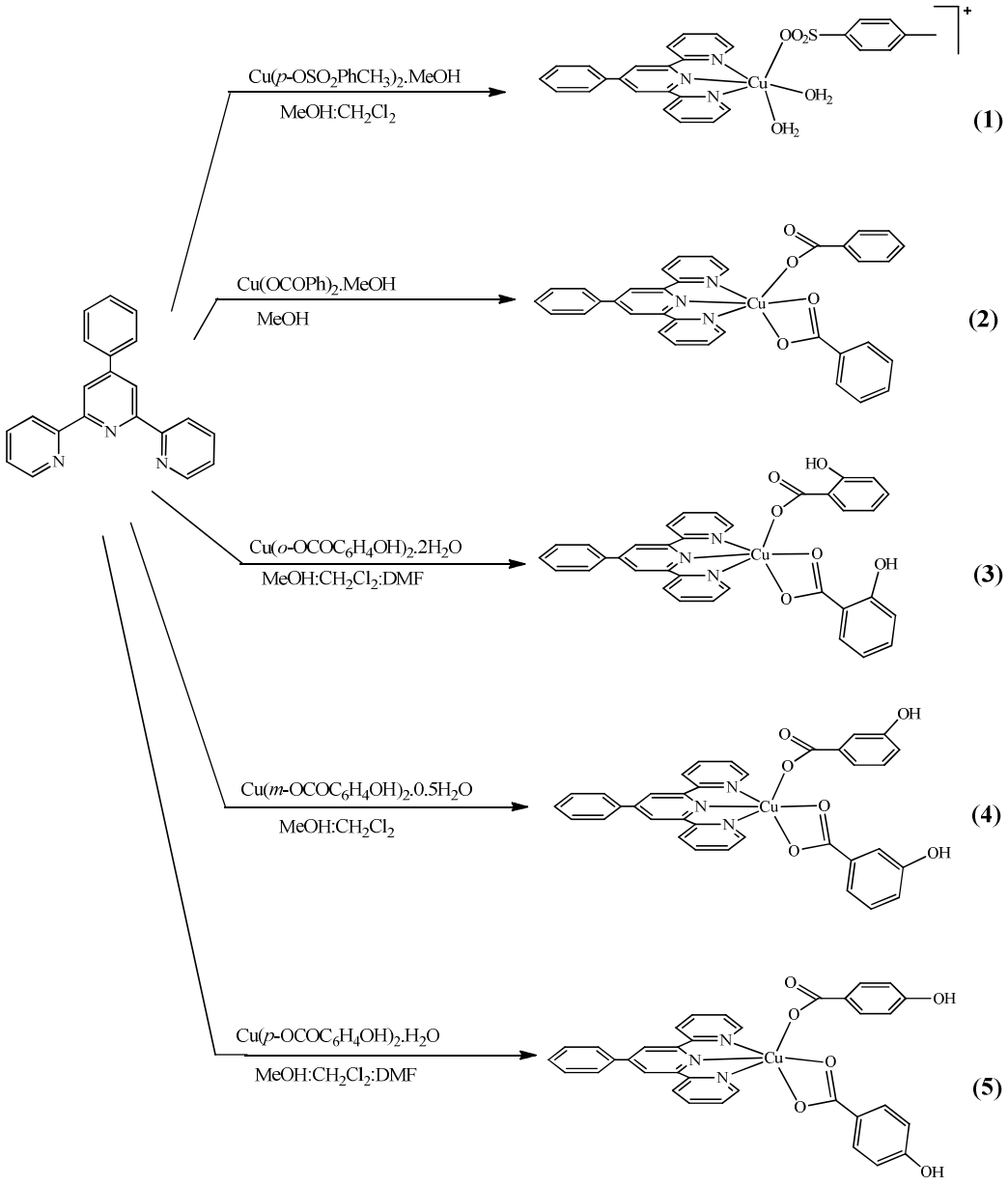

Scheme 1

2.2. Molecular structures of the compounds

Compounds **1** – **5** (Fig. 1 – 5) are mononuclear complexes that crystallized in centrosymmetric space groups with one molecule per each asymmetric unit, for the ionic species **1** also with a *p*-SO_3PhCH_3 counter-ion, and for **4** also with a methanol solvent molecule of crystallization. The molecular geometries involving the Cu1 cations are those of distorted octahedrons with the metals in N_3O_3 environments made of three nitrogen atoms from the terpyridine ligand and three oxygen atoms from two coordinated water molecules and one tolylsulfonate group (**1**), or from the oxygen atoms of carboxylate ligands (**2** – **5**), in each structure one of these acting as a bidentate-chelating donor. This coordination mode is responsible for the pronounced distortion detected in the structures of **2** – **5** as measured by the quadratic elongations of 1.041 – 1.103 and angle variances of 204.34 – 219.30^{o2} (Table 1) [22a]. The chelating carboxylate ligands stand almost perpendicular to the terpyridine moieties, as measured by the angle (denoted as angle *C*, see Table 1) between the least-square plane defined by the atoms CuNNN and that defined by the chelating-bidentate carboxylate ligand, which assume average values of *ca.* 83º. Thus, the equatorial sites in structures **2** – **5** are engaged with the N atoms from terpyridine ligands and one of the O atoms of the chelating carboxylate. This Cu-O bond distance (average *ca*. 1.941 Å, see Table 1) is smaller than the remaining metal-oxygen bonds, what may be a consequence of Jahn-Teller effects. The axial Cu-O bond distances pertaining to the chelating carboxylate ligands (together with the Cu-$O_{sulfonate}$ in **1**) are the longest ones measured in these compounds but still well below the sum of the Van der Waals radii of copper (1.40) and oxygen (1.52).

The results found for the Cu-O bond lengths indicate that the hydroxyl substituent has no obvious effect on this parameter. The Cu–N bond distances (Table 1) range from (average values) 1.995(2) to 2.014(2) Å with the shortest lengths (legends of Figures 1 – 5) pertaining to the $N_{pyridyl}$ atoms in *trans* position to $O_{carboxylates}$. Thus, and as previously found for related zinc compounds, [12b] these distances cannot be related with the pK_a values of the respective conjugated acids, that is, 4.17, 2.98, 4.08 and 4.58 for benzoic, *o*- *m*- and *p*-hydroxyl benzoic acids, respectively.

Moreover, the Cu-O and Cu-N bond distances are in the range usually found for other copper-terpyridine compounds. [23]

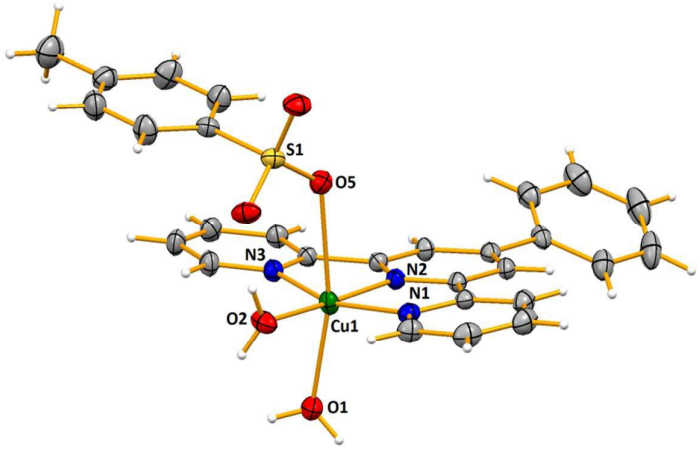

Fig. 1: Thermal ellipsoid plot, drawn at the 30% probability level, of $[Cu(OSO_2C_6H_4CH_3)L(H_2O)_2](OSO_2C_6H_4CH_3)$ (**1**) with atomic numbering scheme. The counterion is omitted for clarity. Selected bond lengths (Å) and angles (°): Cu1–N1 2.0339(16), Cu1–N2 1.9223(16), Cu–N3 2.0304(16), Cu1–O1 2.3182(16), Cu1–O2 1.9490(15), Cu1–O5 2.6189(16); O1–Cu1–N1 86.26(6), O1–Cu1–N2 95.91(6), O1–Cu1–N3 103.43(6), O1–Cu1–O2 87.71(6), O1–Cu1–O5 167.50(5), O2–Cu1–O5 83.05(6).

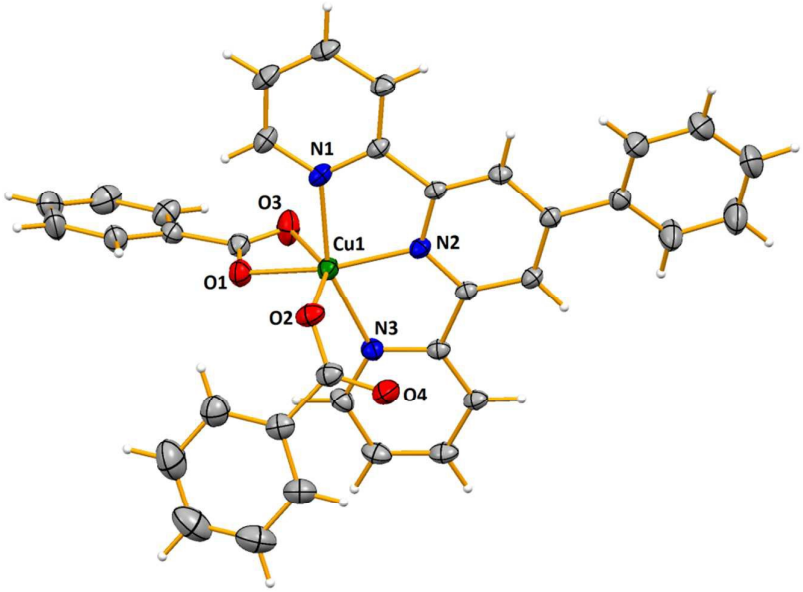

Fig. 2: Thermal ellipsoid plot, drawn at the 30% probability level, of $[Cu(OCOPh)_2L]$ (**2**) with atomic numbering scheme. Selected bond lengths (Å) and angles (°): Cu1–N1 2.0449(17), Cu1–N2 1.9368(16), Cu1–N3 2.0597(17), Cu1–O1 1.9353(15), Cu1–O2 2.2134(16), Cu1–O3 2.763(2); O1–Cu1–N1 96.23(7), O1–Cu1–N2 162.58(7), O1–Cu1–N3 102.15(7), O1–Cu1–O2 99.84(7), O1–Cu1–O3 52.72(6), O2–Cu1–N1 93.62(6), O2–Cu1–N2 97.36(7), O2–Cu1–N3 95.80(6), O2–Cu1–O3 152.48(6), O3–Cu1–N1 91.80(7), O3–Cu1–N2 110.15(6), O3–Cu1–N3 89.20(7), N1–Cu1–N2 79.87(6),

N1–Cu1–N3 157.56(7), N2–Cu1–N3 78.75(6).

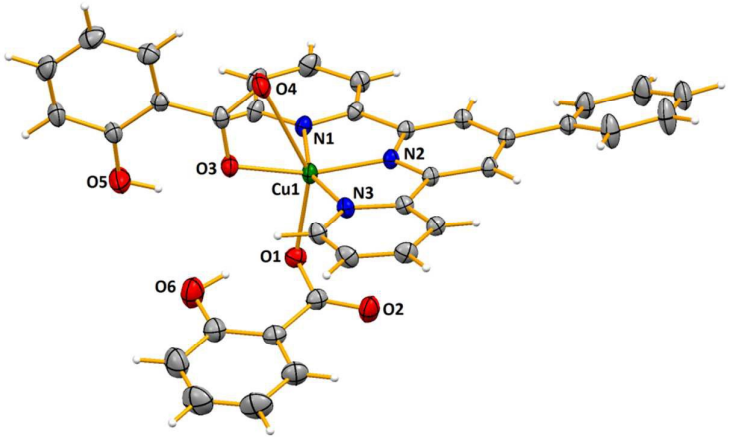

Fig. 3: Thermal ellipsoid plot, drawn at the 30% probability level, of one of the molecules of [Cu(*o*-$OCOC_6H_4OH)_2$L] (**3**) with atomic numbering scheme. Selected bond lengths (Å) and angles (°): Cu1–N1 2.0412(16), Cu1–N2 1.9331(15), Cu1–N3 2.0460(16), Cu1–O1 2.2505(15), Cu1–O3 2.2505(15), Cu1–O4 2.7619(19); O1–Cu1–N1 93.53(6), O1–Cu1–N2 102.06(6), O1–Cu1–N3 96.27(6), O1–Cu1–O3 94.02(6), O1–Cu1–O4 146.90(5), O3–Cu1–N1 96.92(6), O3–Cu1–N2 163.78(6), O3–Cu1–N3 101.04(6), O4–Cu1–N1 91.32(6), O4–Cu1–N2 111.03(6), O4–Cu1–N3 90.65(6), N1–Cu1–N2 80.11(6), N1–Cu1–N3 158.80(6), N2–Cu1–N3 79.52(6).

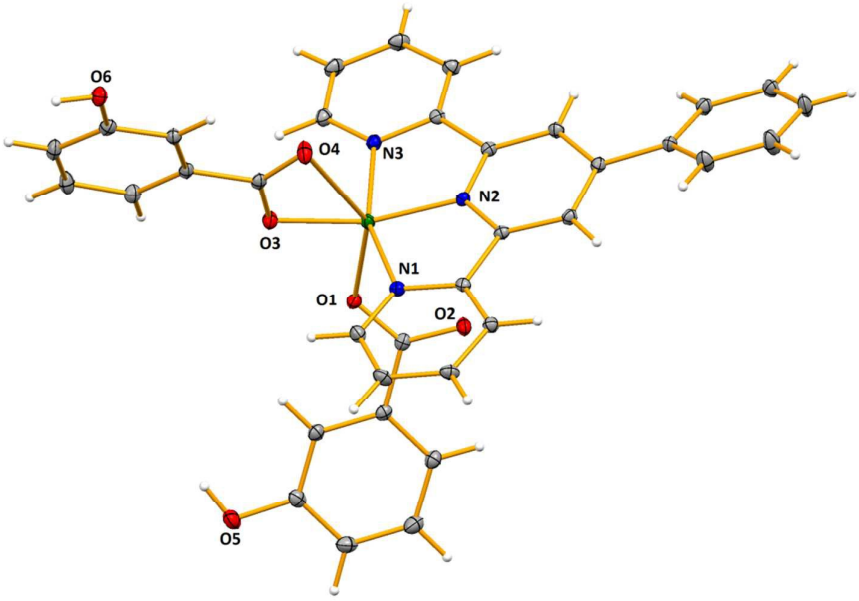

Fig. 4: Thermal ellipsoid plot, drawn at the 50% probability level, of one of the molecules of [Cu(*m*-$OCOC_6H_4OH)_2$L]·CH_3OH (**4**·CH_3OH) with atomic numbering scheme. Methanol molecule is omitted for clarity. Selected bond lengths (Å) and angles (°): Cu1–N1 2.0515(14), Cu1–N2 1.9370(14), Cu1–N3 2.0353(14), Cu1–O1 2.1753(12), Cu1–O3 1.9528(12), Cu1–O4 2.6632(13); O1–Cu1–N1 91.83(5), O1–Cu1–N2 111.01(5), O1–Cu1–N3 98.98(5), O1–Cu1–O3 89.13(5), O1-Cu1-O4 143.13(4), O3-Cu1-N1100.62(5), O3–Cu1–N2 159.80(7), O3–Cu1–N3 97.95(5), N1–Cu1–O4 88.09(5), N2–Cu1–O4 105.18(5), N3–Cu1–O4 94.04(5), N1–Cu1–N3 158.63(6), N2–Cu1–N1 79.24(6),

N2–Cu1–N3 79.68(6).

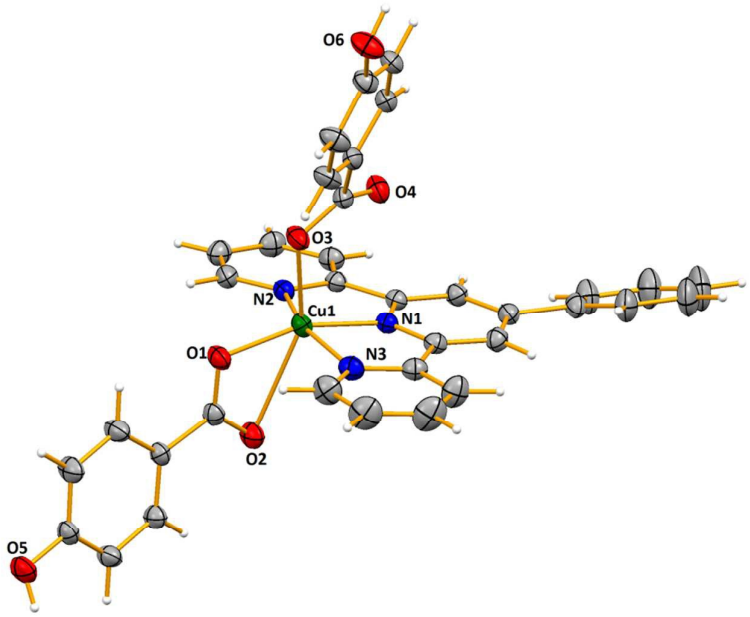

Fig. 5: Thermal ellipsoid plot, drawn at the 30% probability level, of [Cu(*p*-$OCOC_6H_4OH)_2$L] (**5**) with atomic numbering scheme. Selected bond lengths (Å) and angles (°): Cu1–N1 1.9370(14), Cu1–N2 2.0301(15), Cu1–N3 2.0522(16), Cu1–O1 1.9276(12), Cu1–O2 2.6635(14), Cu1–O3 2.2434(13); O1–Cu1–N1 160.24(6), O1–Cu1–N2 100.77(6), N1–Cu1–N2 79.84(6), O1–Cu1–N3 97.13(6), N1–Cu1–N3 79.46 (6), N2–Cu1–N3 158.77(6), O1–Cu1–O3 96.16(5), N1–Cu1–O3 103.02(5), N2–Cu1–O3 102.38(5), N3–Cu1–O3 86.85(6), O1–Cu1–O2 54.94(5), N1–Cu1–O2 105.62(5), N2–Cu1–O2 87.16(5), N3–Cu1–O2 93.90(5), O3–Cu1–O2 150.00(4).

However, the presence and position of the hydroxyl groups conditioned the relative orientations of the monodentate carboxylate moieties towards the chelating-bidentate analogue as measured by the angle (denoted by *MC*, see Table 1) between the least-square planes of these two moieties, which increase in the order *p*-OH (**5**) < *m*-OH (**4**) < *o*-OH (**3**) < H (**2**). That effect can also be quantified by the CuOCC torsion angles (O, C, C atoms belong to the monodentate carboxylate ligand; Table 1) that follow, in magnitude, the same trend. In turn, the angle (denoted by *M*, see Table 1) between the least-square planes of the monodentate ligand and that defined by the CuNNN atoms of the terpyridine ligand increase in the order: *o*-OH (**3**) < H (**2**) < *m*-OH (**4**) < *p*-OH (**5**). The twisting of the phenyl ring of the terpyridine

ligands is also affected by the type and nature of the coligands as denoted by the angle (denoted by *T*, see Table 1) between the least-square plane defined by the CuNNN atoms and that defined by the terpyridine substituent; the highest value was found for **1** (25.11º) and the shortest one for **2** (12.17º).

Table 1 – Selected crystallographic features of structures **1** – **5**.

	1	**2**	**3**	**4**	**5**
QE (Å)[a]	1.044	1.103	1.102	1.091	1.090
AV (º²)[a]	65.65	219.38	219.36	219.25	204.45
Avg. Cu-N	1.995(2)	2.014(2)	2.007(2)	2.008(1)	2.006(2)
$Cu–O_{equatorial}$ (Å)	1.9490(15)	1.9353(15)	1.9393(13)	1.9528(12)	1.9276(12)
$Cu–O_{water(or\ carbo)}$ (Å)	2.3182(16)	2.2134(16)	2.2505(15)	2.1753(12)	2.2434(13)
$Cu–O_{sulfo(or\ carbo)}$ (Å)	2.6189(16)	2.763(2)	2.7619(19)	2.6632(13)	2.6635(14)
∠ *T* (º)[b]	25.11	12.17	14.14	21.41	20.19 (29.39)[c]
∠ *C* (º)[b]	-	83.58	85.64	78.64	84.92
∠ *M* (º)	10.18	20.30	16.28	58.52	71.40
∠ *MC* (º)[d]	-	79.02	78.09	45.47	32.94
CuOCC torsion in monodentate ligand	-	-91.95	103.03	146.44	-153.44

[a] QE = quadratic elongation; OV = angle variance [22].

[b] Angle between the least-square plane defined by the Cu-N-N-N atoms and that defined by the phenyl substituent of terpyridine (*T*), or the chelating-bidentate carboxylate ligand (*C*) or the monodentate (carboxylate or sulfonate) ligand (*M*).

[c] Value obtained for the phenyl group in disordered position.

[d] Angle between the least-square planes defined by the chelating-bidentate and the monodentate carboxylate ligands.

Intermolecular π···π stacking interactions could also be found in these structures (Figure S1 of Supplementary Material file), the strongest values found for **2** – **5** (in the 3.569 – 3.651 Å range and involving solely the pryridyl rings) suggesting a perfect (face-to-face), or slightly offset, stack whose accepted values fall in the 3.3 – 3.8 Å range.[22b] Resulting from the presence of water ligand molecules (in **1**) and the

special positions of the hydroxyl groups (in **3** – **5**) the compounds are involved in medium-strong hydrogen bond interactions (Table S1 and Figure S2 of Supplementary Material file) that lead to infinite 1D chains (in **1** and **4**) and to an infinite 2D network (in **5**). In complex **3**, intramolecular contacts between the *o*-OH group and the metal bound *O*-carboxylates are established, leading to 6-membered H-bond rings.

2.3. TG-DTA and conductivity properties of the complexes

The TG properties of complexes **1** – **5** were studied and are exemplified in Fig. 6 for compounds **1** and **2** (see also Figures S3 – S5 in Supporting Material file). In **1** the step in the range of 95-140 °C (centred at *ca*. 120 °C) should concern the release of the two coordinated water molecules with weight loss of 4.5 % (calc. 4.8 %). The obtained product is stable until *ca*. 375 ºC and then decomposes with no evident intermediate steps in the TG analysis until stabilization at the temperature of 778 °C. However, in the DTA plot two clear decomposition processes are detected, the former between 325 and 430 ºC (centred at *ca*. 375 ºC), and the latter between 430 and 580 ºC (centred at *ca.* 535 ºC) and corresponding to weight losses of *ca.* 23 and 42 % consistent with the release of tolylsulfonate and terpyridine ligands, respectively. The final product weights 12.7 % of the initial compound **1** sample, being consistent with CuO (calculated value of 10.6 %).

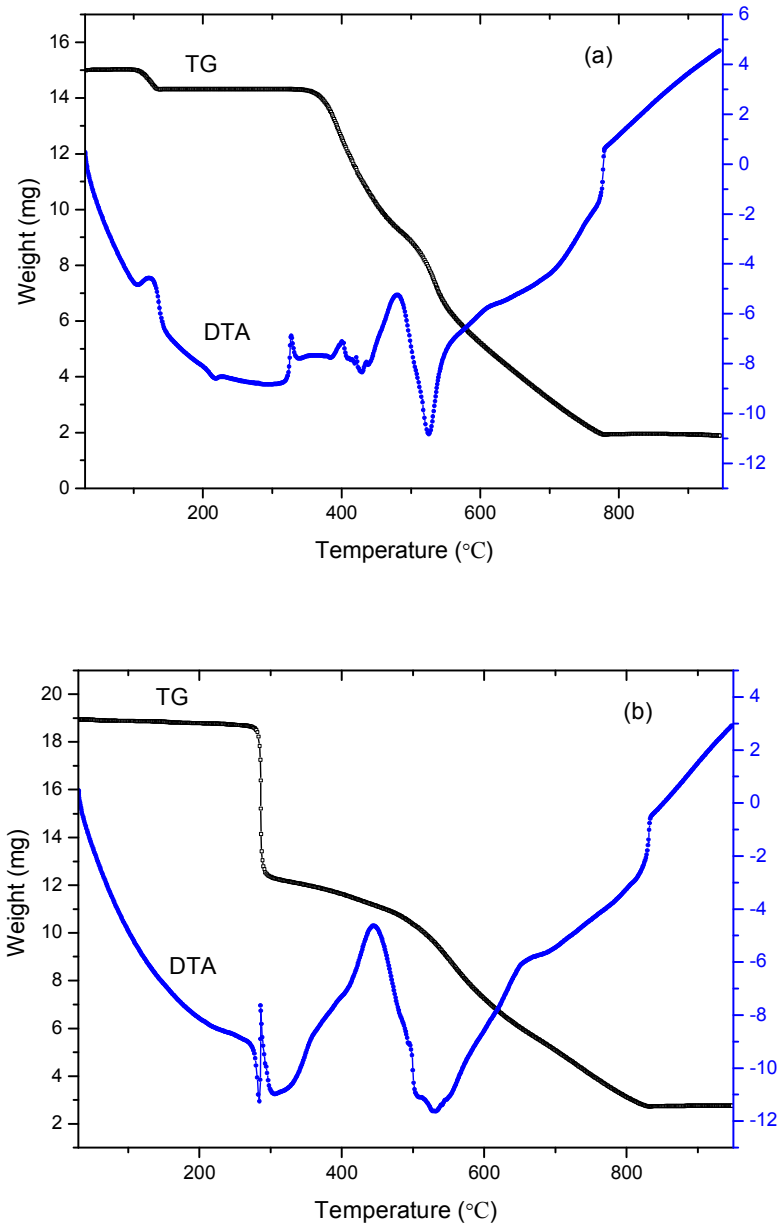

Fig. 6: Thermal analyses (TG and DTA plots) of complexes **1** (a) and **2** (b).

The TG and DTA curves of compound **2** are shown in Fig. 6(b). The fast weight loss of 35.1 % at 294 °C can be accounted for by the loss of the two benzoate ligands (a calculated value of 34.8 % is obtained if a CO group remains coordinated to the metal). Decomposition steps occur in the range of 300 – 525 °C with the decrease in 14 % in weight being due to the loss of the phenyl group of terpyridine.

The total weight loss of 50.4 % from 300 until 832 °C concerns the decomposition of the terpyridine ligand of the complex (theoretical loss of 50.3 %). The final product weight is 14.4 %, which is comparable to the calc. value of 12.9 % for CuO.

The TG-DTA properties of the benzoate complexes **3**, **4** and **5** were also studied and their decomposition processes are summarized in Table 2 (Figures S3 - S5 for the respective plots, in Supplementary Material file). The final product of the thermal decomposition of these complexes is also CuO, what corresponds to 13.4 % for **3**, 11.9 % for **4** and 12.4 % for **5**, complying with the respective theoretical value of 12.3 %, 12.0 % and 11.4 %.

The TG-DTA results indicate that the highest temperature (in ºC) at which the compounds preserve their integrity vary in the order **1** (390) > **2** (300) > **4** (271) ≥ **3** (260) > **5** (230). The decomposition processes in all the compounds appear to follow a similar trend starting by losing the crystallization solvent molecules, followed by the anionic ligands and ultimately undergoing terpyridine decomposition. The final stable temperatures (in ºC) vary in the order **2** (832) ≥ **3** (828) > **1** (778) > **5** (711) > **4** (692).

The molar conductance (Λ_M) of 10^{-3} M DMSO solutions of compounds **1-5** were also determined. The value for **1** (33 $\Omega^{-1}cm^2mol^{-1}$) is in agreement with those found for 1:1 electrolytes in this solvent[24] which further confirms the ionic nature of this compound in solution. For compounds **2**, **4** and **5** the achieved values (*ca*. 9.5 Ω^{-1} cm^2mol^{-1}) are too low to account for ionic nature, and therefore they confirm that these complexes are neutral in solution.

However, although the solid state structure of **3** indicates that it is neutral, the conductivity in DMSO (25 $\Omega^{-1}cm^2mol^{-1}$) may indicate a partial dissociation, with possible coordination of solvent molecules and the establishment of an equilibrium involving neutral and ionic species. Such a unique behaviour of complex **3** conceivably can be accounted for by the establishment of H-bonding between the *ortho*-OH substituent of the benzene ring and an O atom of the carboxylate group as disclosed by X-ray analysis, with a resulting increase of the ligand labilization towards displacement by a solvent molecule.

Table 2 - Decomposition processes in TG-DTA of the benzoate complexes **3 – 5**.[a]

Complex	T range (ºC)	Weight loss (%)	Assignment of the released fragment
3	**260** – 300	24.6	Hydroxybenzoate
	300 – 539	23.1	Hydroxybenzoate
	539 – 828	35.0	Terpyridine
4	T_i – 100	2.5	Half methanol molecule
	271 – 388	38.3	Hydroxybenzoates
	388 – 692	47.3	Terpyridine
5	T_i – 146	7.5	1.3 acetonitrile molecules
	230 – 410	42.6	Hydroxybenzoates
	410 – 711	38.0	Terpyridine

[a] The numbers in bold refer to the temperature at which the complex starts to decompose. T_i = initial temperature.

2.4. Biological activities

Compounds **1**–**5** were screened for the *in vitro* tumour-inhibiting activity against two different human cancer cell lines, a colorectal carcinoma cell line (**HCT116**) and a hepatocellular carcinoma cell line (**HepG2**), and also against a normal fibroblast cell line using the MTS metabolic assay. After 48 h of incubation we observed a decrease of the cell viability, in a dose-dependent manner, for all compounds in HCT116 and HEPG2 tumour cell lines (Figures 7 and 8).

The compounds more active against both tumour cell lines were **1** and **4** with IC_{50} values of 0.066 ± 0.05 μM (HCT116) and 0.241 ± 0.015 μM (HepG2) for compound **1** and 0.437 ± 0.094 μM (HCT116) and 0.535 ± 0.033 μM (HepG2) for compound **4** (Figures 7 and 8 and Table 3).

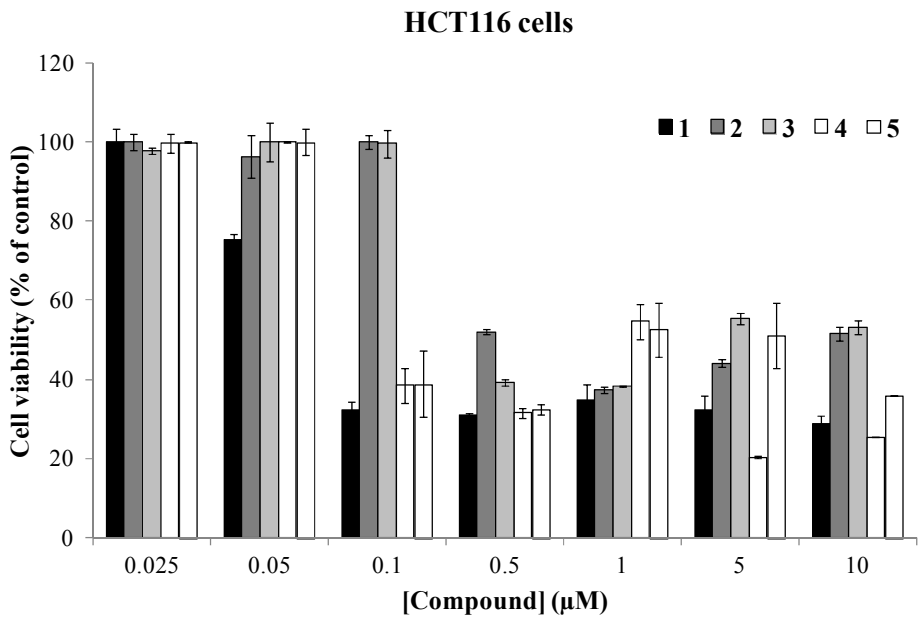

Figure 7 - Dose-dependent cytotoxicity of the copper compounds **1** – **5** in HCT116 cells. Cells were incubated in the presence of the compounds for 48 h and their viability was evaluated by MTS assay. The results are expressed as the mean ± SEM percentage compared to controls from three independent experiments.

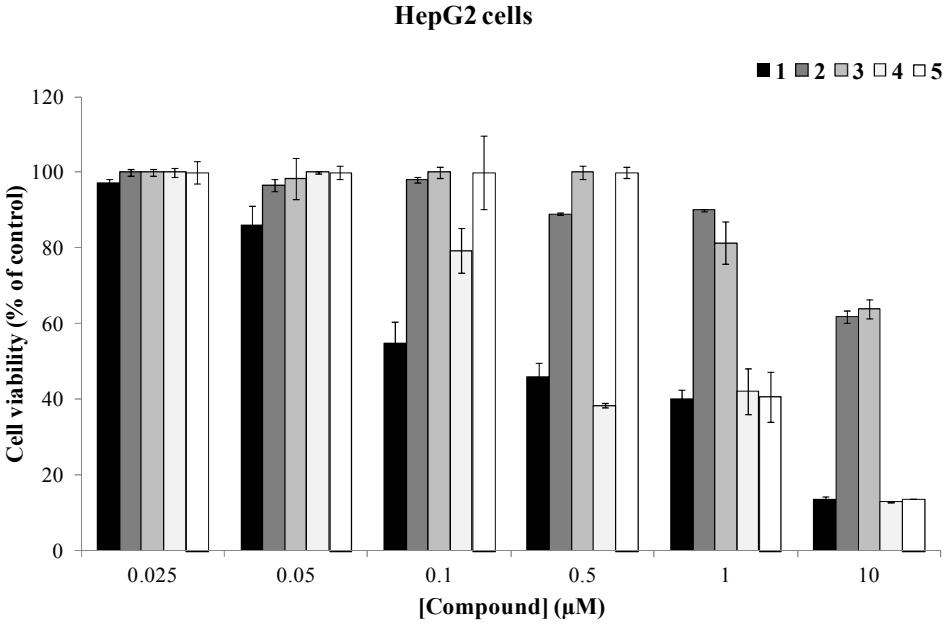

Figure 8 – Dose-dependent cytotoxicity of the copper compounds **1** – **5** in HepG2 cells. Cells were incubated in the presence of the compounds for 48 h and their viability was evaluated by MTS assay. The results are expressed as the mean ± SEM percentage compared to controls from three independent experiments.

Table 3 - IC_{50} values calculated by nonlinear regression analysis using GraphPad Prism (Graph Pad Software Inc, San Diego) for compounds **1** – **5** in HCT116 and HepG2 tumour cell lines and in normal human fibroblasts.

Compounds	*HCT116* IC_{50} *(μM)*	*HepG2* IC_{50} *(μM)*	*Normal Human Fibroblasts* IC_{50} *(μM)*
1	0.066 ± 0.05	0.241 ± 0.015	5.483 ± 0.003
2	0.312 ± 0.03	14.04 ± 0.5	>20
3	0.468 ± 0.006	13.61 ± 0.5	>20
4	0.437 ± 0.094	0.535 ± 0.033	>5
5	1.490 ± 0.165	0.735 ± 0.114	>5

It should be noted that compounds **1** and **4** present lower IC_{50} values for HCT116 tumour cells than the common antitumour drugs cisplatin (4.14 μM)[24] and doxorubicin (1.4 μM)[25]. With the exception of compound **5** all the other tested compounds are more cytotoxic against HCT116 colorectal carcinoma compared to HepG2 hepatocellular carcinoma (Figs. 7 and 8 and Table 3).

The cytotoxicity of compounds **1** - **5** in normal fibroblasts was also evaluated and the IC_{50} values were above 5 μM for all compounds (Fig. 9, Table 3 and results not shown). For compounds **4** and **5** the dose dependent results of the viability assays in fibroblasts were similar to those presented for compound **1** and in this regard they are not shown in Fig. 9. As we can observe in Fig. 9 compound **1** is 83 and 23 times more cytotoxic for HCT116 and HEPG2 tumour cells, respectively comparing with normal fibroblasts (Figs.7, 8, 9 and Table 3).

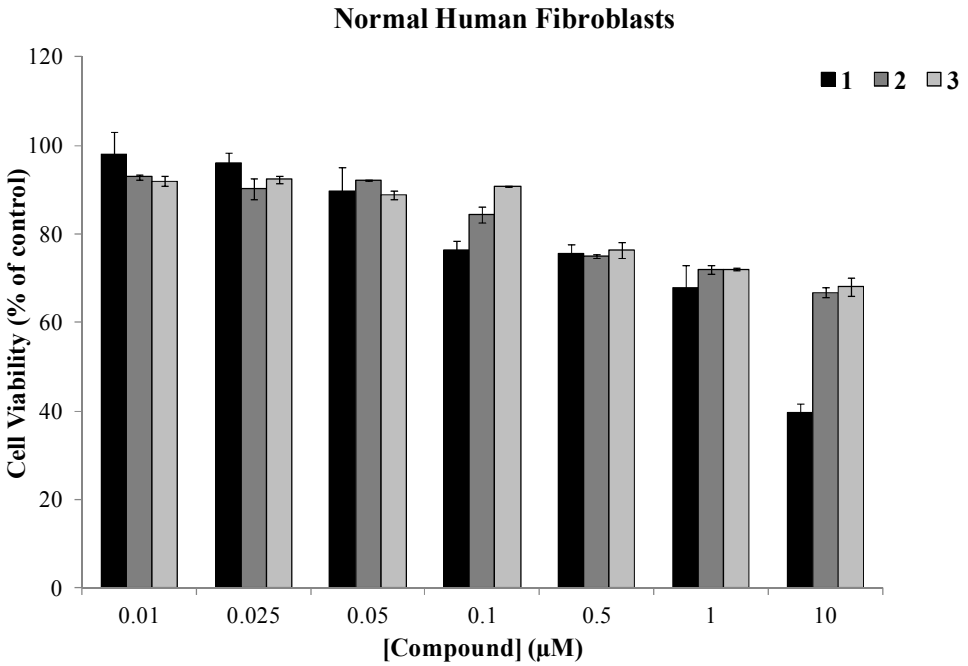

Figure 9 – Dose-dependent cytotoxicity of the copper compounds **1**, **2** and **3** in normal fibroblasts. Cells were incubated in the presence of the compounds for 48 h and their viability was evaluated by MTS assay. The results are expressed as the mean ± SEM percentage compared to controls from three independent experiments. For compounds **4** and **5** the results were similar to those presented for compound **1** and are not represented.

Moreover, all the five compounds studied show higher cytotoxicity against tumour cell lines, particularly HCT116 carcinoma cell line, as compared to normal fibroblasts. Indeed, the highest concentration tested for compounds **2** and **3** (10 μM) allows to maintain 68 % of the fibroblasts viable (Fig. 9). Compounds **1**, **4** and **5** have a higher cytotoxicity in fibroblasts; nevertheless, at the concentration corresponding to the IC_{50} for the HCT116 tumour cell line there are 94.2 % of viable fibroblasts. Although HCT116 and HepG2 are epithelial type tumour cells, this result is very promising and viability assays will be also carried out in normal epithelial cell lines in order to confirm particularly the higher cytotoxicity of compounds **1**, **4** and **5** to tumour cell lines, in particular colorectal carcinoma cell lines. Also as observed in Supplementary Figure S6 all five compounds are stable when incubated for 24 h in PBS at 37ºC (to mimic biological assays conditions).

The higher antiproliferative potential observed for compound 1 compared to the other four compounds may in part be related with its positive charge and the more labile ligand (water) compared with the neutral compounds 2-5. As previously described for other positively charged copper(II) complexes cellular internalization may be supported by human copper transporters (hCtr), or other cellular transporters which can transfer positively charged molecules [26].

In order to underline the cell death mechanism behind the anti-proliferative effect of compound **1** in tumour cell lines, Hoechst 33258 staining was performed. It is known that Hoechst is able to stain all nuclei, emitting blue fluorescence when bonded to nucleic acids[27]. It is possible to observe nuclear changes such as chromatin condensation and nuclear fragmentation, that are typical features of apoptosis[27-28]. While viable cells exhibit a fluorescence uniformly distributed throughout the nucleus and no changes in chromatin, apoptotic cells, on the other hand, show chromatin condensation, which results in smaller nuclei with enhanced fluorescence when compared to normal cells[27;29]. The effect of compound **1** in both HCT116 and HepG2 cells is shown in Figure 10, in which the presence of cells with apoptotic features correlates to the increase in the compound concentration, demonstrating its ability to induce apoptosis, observation not seen with the vehicle control (DMSO; A and E), that does not change nucleus morphology.

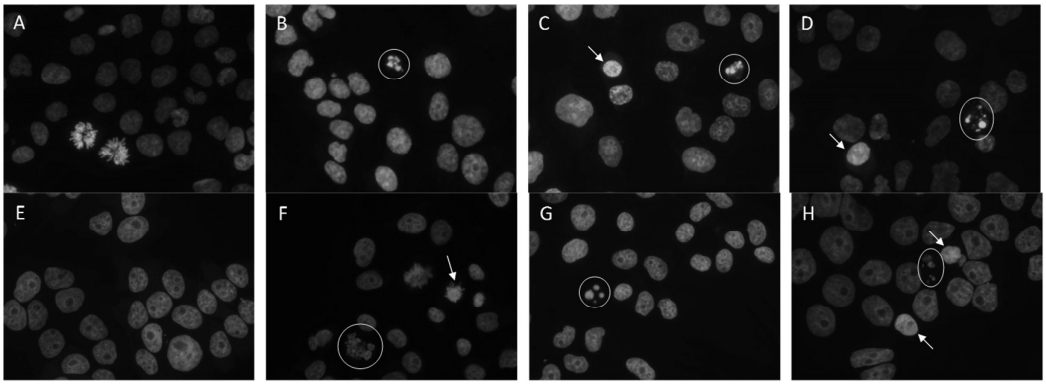

Figure 10 – Apoptosis induced by compound **1** in HCT116 (A-D) and HepG2 (E-H) cells staining with Hoechst 33258. Control with DMSO (0.1% (v/v); A and E), 0.025 µM of compound **1** (B and F), 0.05 µM of compound **1** (C and G) and 0.1 µM of compound **1** (D and H). Circles represent nuclear fragmentation and the arrows chromatin condensation.

To corroborate the observed results, double staining with Annexin V-FITC and propidium iodide was performed on HCT116 tumour cells. Annexin V binds to phosphatidylserine that is externalized in early apoptosis, constituting a typical event in apoptosis[27; 30-32]. On the other hand, PI binds to nucleic acid of cells with compromised cell membrane, thus staining cells in late apoptosis or necrotic cells[32; 33]. HCT116 cells treated with compound **1** revealed a considerable decrease of viable cells relative to control (more than 50 %) and cells were mostly in late apoptosis (Figure 11 and Table 4). Only few cells were detected in necrosis as leading to the consideration that the main mechanism of action of compound **1** is through the induction of apoptosis (Figure 11 and Table 4).

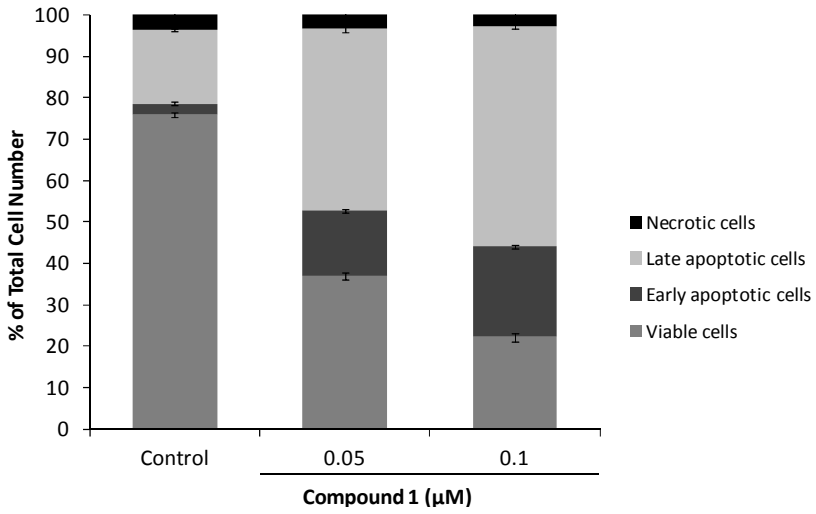

Figure 11 - Double staining with Annexin V-FITC and PI in HCT116 tumour cells exposure for 48 h to DMSO (0.1% (v/v); control), 0.05 or 0.1 μM of compound **1**. Cell death was determined by flow cytometry and the results were analysed in *Attune® Cytometric software*.

Table 4 - Percentage of viable, early apoptotic, late apoptotic and necrotic cells after incubation of HCT116 cells with DMSO (control), 0.05 or 0.1 μM of compound **1**. Values are referent to data presented in Figure 11, and expressed as the mean ± SEM percentage from three independent experiments.

	Control (DMSO)	[Compound 1] (μM)	
		0.05	0.1
Viable cells	76 (± 4.3)	37 (± 7.6)	22 (± 4.5)
Early apoptosis	3 (± 0.3)	16 (± 3.4)	22 (± 7.7)
Late apoptosis	18 (± 5.0)	44 (± 10.7)	53 (± 3.5)
Necrosis	3 (± 0.5)	3 (± 0.3)	3 (± 0.6)

On the basis that compound **1** is able to induce apoptosis, the expression level of genes involved in cell death mechanism was analysed, namely *BAX*, *BCL-2* and *CASP3* encoding for Bax, Bcl-2 and caspase 3 proteins, respectively (Figure 12). It is known that the intrinsic pathway of apoptosis is regulated by Bcl-2 family of proteins which is composed by two groups: pro-apoptotic proteins, including Bax, and anti-apoptotic proteins, including Bcl-2[34]. These proteins regulate the apoptotic process: anti-apoptotic members block the release of cytochrome c whereas pro-apoptotic members stimulated its release. The occurrence of apoptosis is a process highly dependent on the ratio between Bcl-2 and Bax rather than just the levels of Bcl-2[35].

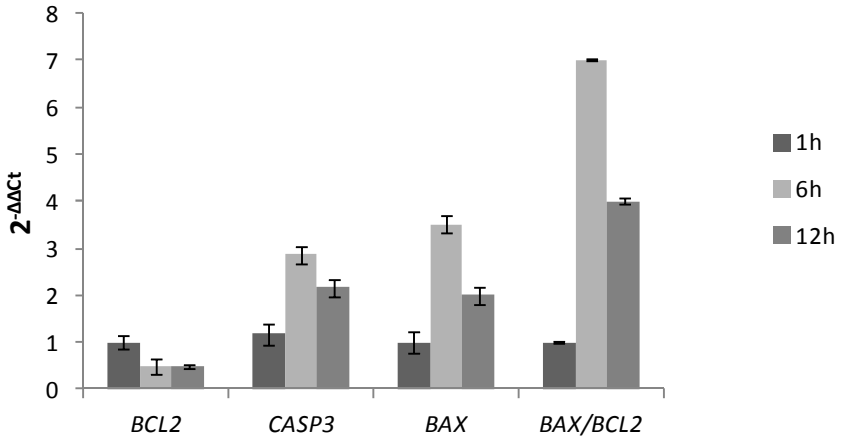

Figure 12 - Expression of apoptotic genes *BCL-2*, *BAX*, *CASP3* in HCT116 cells incubated with 0.05 μM of compound **1** during 1, 6, and 12 h. Variation of gene expression is calculated by $2^{-\Delta\Delta Ct}$ and the data is presented as alteration in gene expression, normalized to an internal reference (*rRNA18S5* gene) and untreated control (0.1 % (v/v) DMSO).

After 1 h of incubation with compound 1, the ratio *BAX*/*BCL-2* was 1, showing that expressions of *BCL-2* and *BAX* are equivalent, indicating that the apoptotic process is not active (Figure 12). However, over time, the ratio *BAX*/*BCL-2* increased (7 for 6 h of incubation and 4 for 12h of incubation), correlating with the increased expression of *BAX* and decreased of *BCL-2* that can be associated to the increase in apoptotic cells (Figure 12). Also *CASP3* encoding caspase 3, an effector caspase, shows a time dependent increase at the level of mRNA (Figure 12). Indeed, as the activation of Caspase 3 is dependent on the increase of BAX/BCL-2 ratio, it was observed that the expression of *CASP3* increases considerably (at incubation times between 6 and 12 h). The obtained data indicate that the apoptotic process is active at 6 h (more expression of BAX compared to BCL-2) and progression of apoptosis is still observed after 12h (related to the decrease of *BCL-2*, stabilization of *BAX* and increased expression of *CASP3*) (Figure 12). Hence, it is assumed that compound 1 indeed triggers apoptosis.

It is known that a transition metal complex can bind to DNA via both covalent and/or non-covalent interactions[36]. Non-covalent interactions include intercalation between the bases, and for instance binding to major groove, minor groove and sugar–phosphate backbone[37].

In order to access the binding capability of complexes **1-5** to CT-DNA, absorption spectroscopy was used (Figure 13).

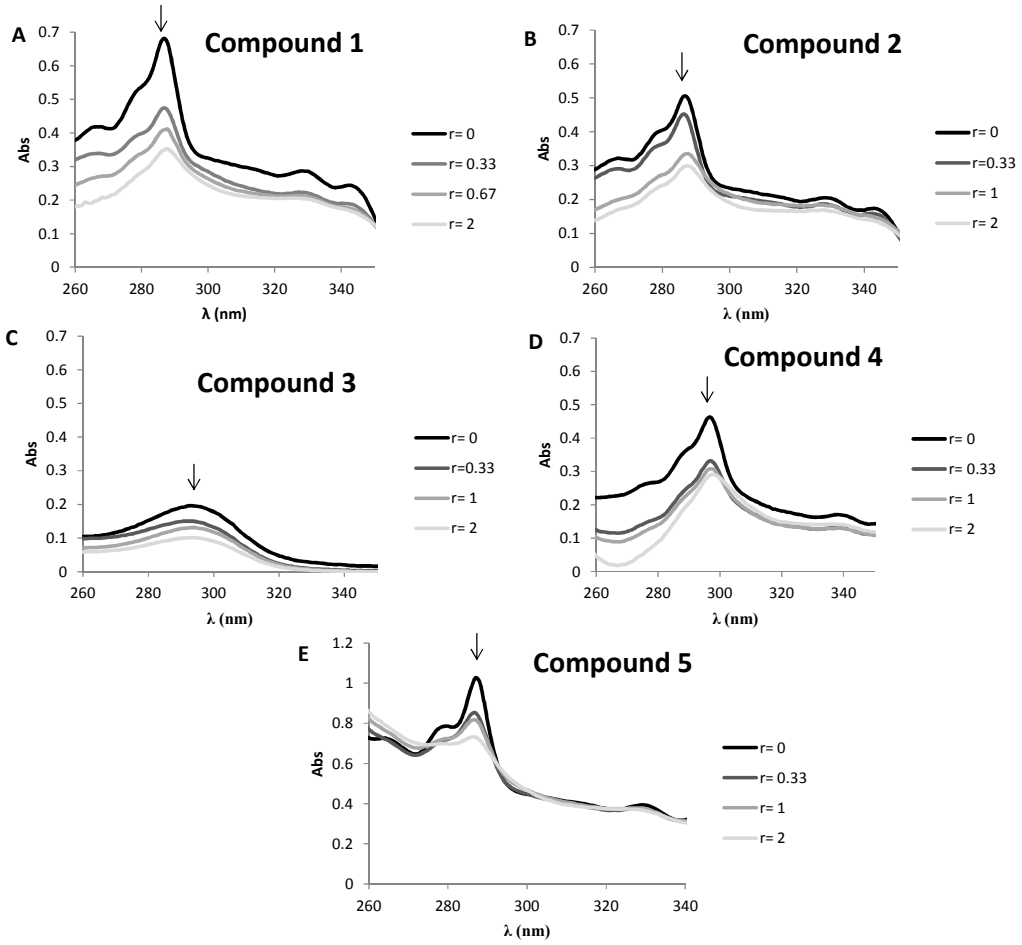

Figure 13- Variation of absorbance spectra of compounds **1-5** (15 μM) in the absence (black line, r = [DNA]/[Compound] = 0) and in presence of increasing concentrations of CT-DNA (5 to 30 μM; r= 0.33-2) (gray lines; the highest DNA concentration represented by the lighter grey line – r = 2). Spectra were taken in buffer 5 mM Tris-HCl, 50 mM NaCl (pH 7.2). The arrow indicates the variation in absorbance with increased concentration of CT-DNA. Results were used, accordingly to equation 3 in Experimental section (sub-section 3.4) to determine the binding constant for DNA (K_b).

With increasing concentration of CT-DNA, the absorption bands of the compounds are affected, resulting in the tendency of hypochromism and a minor red shift which is observed in all the complexes (Figure 13). Hypochromism results from the contraction of DNA in the helix axis, as well as from the conformational change of DNA[38]. The electronic absorption spectra of the compounds in 5mM Tris-HCl and 50 mM NaCl buffer (pH 7.2) are similar in shape and exhibit an intense absorption band in the UV region (287 nm for compounds **1**,**2**, **4** and **5**; 295 nm for compound **3**) (Figure S7 supplementary material). This band is attributed to intraligand π-π* transition of the coordinated groups. The increase in the concentration of CT-DNA results in a minor red shift in the range ~ 1.5 nm and significant hypochromicity. The observable hypochromism and red shift are usually characterized by the non-covalently intercalative binding of the compound to the DNA helix, due to the stacking interaction between the aromatic rings of the compound and base pairs of DNA[39,40]. This small bathochromism result might be due to the decrease in the energy of the transition, when the π-orbital of the base pairs of DNA coupled with the π* orbital of the intercalated ligand. The intrinsic binding constants (K_b) of the metal complexes with CT-DNA were obtained by monitoring the changes in the intraligand band with increasing concentration of DNA (Figure 13 and Table 5).

Table 5 - Intrinsic binding constants (K_b) of the compounds **1-5** with CT-DNA obtained by monitoring the changes in the intraligand band with increasing concentrations of CT-DNA (5-30 μM). Values are referent to data presented in Figure 13, and expressed as the mean ± SEM percentage from three independent experiments.

Compound	K_b (± SEM) (M^{-1})
1	1.25 (± 0.02) x10^5
2	1.5 (± 0.03) x10^5
3	1.5 (± 0.01)x10^6
4	1.0 (± 0.02)x10^6
5	1.4 (± 0.02)x10^5

The binding constant values, K_b determined for compounds **1**, **2**, **3**, **4** and **5** are lower (Table 5) than the one determined for the classical DNA intercalator ethidium bromide (ET) ($7x10^7$ M^{-1})[41], indicating that these compounds have much less ability to intercalate DNA compared to ET. Interestingly, the K_b values observed for compounds **3** and **4** are 10 times higher than the ones observed for compounds **1**, **2** and **5** (Table 5). These results *per se* cannot be correlated with the antiproliferative potential of compounds. Indeed, in HCT116 cells the antiproliferative potential of compound **1** is clearly higher than that of compound **5**. Interestingly, when we compare the angle (denoted by *M* in Table 1) between the least-square planes of the monodentate ligand and that defined by the CuNNN atoms of the terpyridine ligand, as previously stated, it increases in the order: *o*-OH (**3**) < *m*-OH (**4**) < *p*-OH (**5**), possibly favouring compound **3** to access and intercalate the DNA helix.

In order to evaluate the effect of compound **1** in the *in vitro* DNA cleavage, pDNA was incubated with different concentrations of compound **1** during 24 h (Figure 13). A decrease of the SC form and an increase of the linear (L) form were observed. The NC form has no significant variations over time, assuming that SC is converted directly into the L form indicating that compound **1** causes double-strand pDNA cleavage (Figure 14).

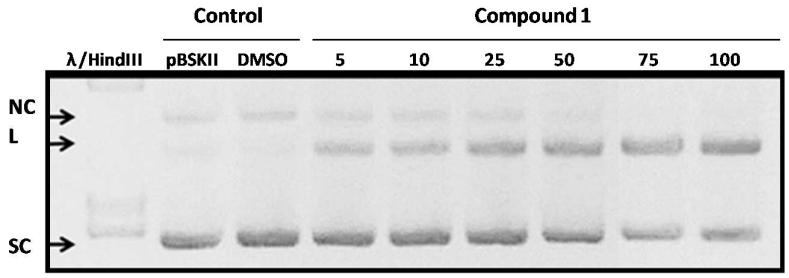

Figure 14 – Agarose gel electrophoresis (0.7 % (w/v)) of pBSK II DNA (200 ng) incubated without (control) or with compound **1** (5-100 μM) for 24 h at 37 °C in 5mM Tris-HCl and 50 mM NaCl buffer (pH 7.2). Lane 1: λ/HindIII molecular marker; Lane 2: pBSK II control; Lane 3: pBSK II incubated with 3% (v/v) DMSO; Lanes 4-9: pBSK II incubated with increasing concentrations of compound **1** (5, 10, 25, 50, 75 and 100 μM). SC – supercoiled form; NC – nicked circular form; L – linear form.

Also the incubation of pBSK II with 10 or 50 μM of compound **1** between 1 h and 48 h shows a time dependent decrease of the SC form and an increase of linear (L) form (Figure 15). The L form presents a gradual increase over time that appears to include the decay of SC and NC forms indicating that both are converted in L conformation (Figure 15). Since the NC form does not increase, it is assumed that the SC is converted directly in L, indicating as previously that compound **1** induces *in vitro* a pDNA double-strand cleavage (Figure 15).

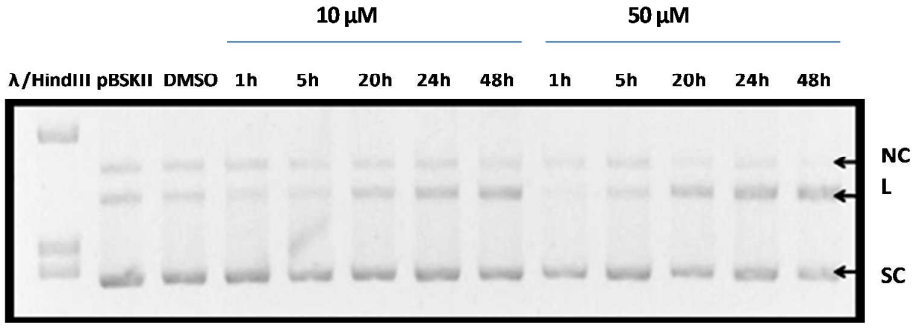

Figure 15 - Agarose gel electrophoresis (0.7 % (w/v)) of pBSK II DNA (200 ng) incubated at 37 °C in 5mM Tris-HCl and 50 mM NaCl buffer (pH 7.2) with compound **1** at different time periods. Lane 1: λ/HindIII molecular marker; pBSK II control; Lane 3: pBSK II incubated with 3% (v/v) DMSO; Lanes 4-8: pBSK II incubated with 10 μM compound **1** at 1, 5, 20, 24 and 48 h. Lanes 9-13: pBSK II incubated with 50 μM compound **1** at 1, 5, 20, 24 and 48 h. SC – supercoiled form; NC – nicked circular form; L – linear form.

The ability of the other compounds **2-5** to induce *in vitro* double-stranded pDNA cleavage was also studied. In this regard, pUC 18 was incubated in the presence or absence of each compound during 24 h at 37ºC. As already shown for compound **1** (Figures 14-16), compounds **2-5** are able to cleave *in vitro* pDNA without the addition of H_2O_2 to the reaction medium. An increase of the linear (L) form with the increase of compound concentration was observed for all compounds particularly for **2** and **5** (Figure 16). Concomitant with this increase, a decrease in SC form is observed assuming that SC is converted directly into the L form indicating that the other compounds can also induce double-strand pDNA cleavage (Figure 16).

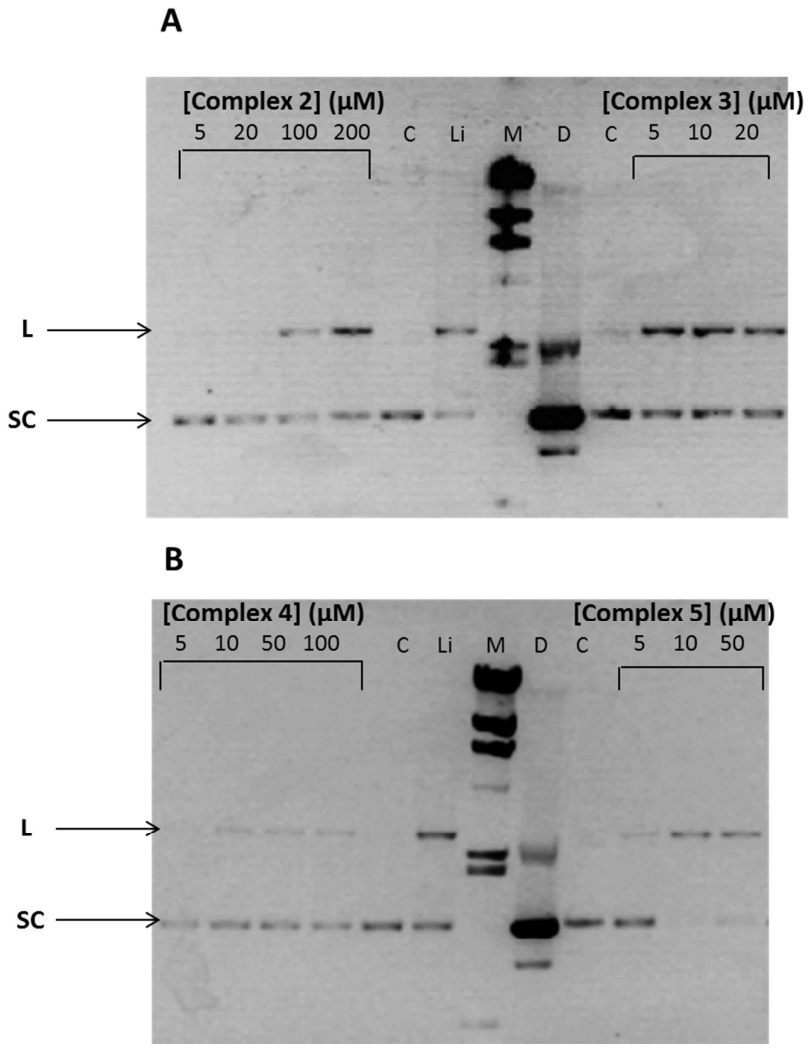

Figure 16 – Agarose gel electrophoresis (0.7 % (w/v)) of pUC18 DNA (200 ng) incubated without (control) or with **A)** compounds **2** (5-200 μM) and **3** (5-20 μM) and **B) 4** (5-100 μM) and **5** (5-50 μM) for 24 h at 37 °C in 5mM Tris-HCl and 50 mM NaCl buffer (pH 7.2). M - λ/HindIII molecular marker; D – pUC18 control; Li – pUC18 partially digested with *EcoRI* for 2h; C - pUC18 incubated with 3% (v/v) DMSO. SC – supercoiled form; L – linear form.

Interestingly, besides the 10 times higher affinity towards CT-DNA of **3** compared to **4** and **5**, that compound is able to induce pDNA cleavage at lower concentrations (at 5 μM an high increase in the L form is already observed). The *ortho* position of the hydroxyl groups in compound **3** may eventually favour this cleavage process (see above the structural description).

Copper complexes are capable to break DNA by hydrolytic mechanisms, but it has also been reported that these types of complexes have the ability to generate reactive

oxygen species (ROS) in the presence of a reductant and dioxygen to induce oxidative cleavage of DNA[42;43].

In this regard, we assessed the mechanism of this *in vitro* pDNA cleavage using compound **1** as a model (Figure 17).

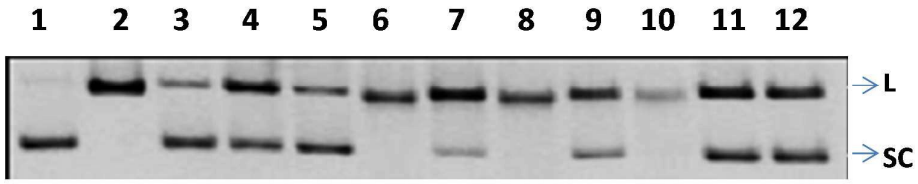

Figure 17 – Agarose gel electrophoresis (0.7 % (w/v)) of pUC18 DNA (200 ng) incubated with compound **1** (50 μM) in the presence or absence of H_2O_2 (2 mM) and reductants. Lane 1: pUC18 DNA; Lane 2: pUC18 linearized with *EcoRI*; Lane 3: pUC18 with 3 % (v/v) DMSO; Lane 4: pUC18 incubated with compound **1**; Lane 5: pUC18 incubated with H_2O_2; Lane 6: pUC18 incubated with compound **1** and H_2O_2; Lane 7: pUC18 incubated with compound **1** and NaN_3 (25 mM); Lane 8: pUC18 incubated with compound **1**, H_2O_2 and NaN_3; Lane 9: pUC18 incubated with compound **1** and DMSO (100mM); Lane 10: pUC18 incubated with compound **1**, H_2O_2 and DMSO; Lane 11: pUC18 incubated with compound **1** and EDTA (25mM); Lane 12: pUC18 incubated with compound **1**, H_2O_2 and EDTA. SC – supercoiled form; L – linear form.

As shown in Figure 17, pDNA cleavage by compound **1** is enhanced in the presence of H_2O_2 and only the L form is visualized (Lane 6 *vs*. Lane 4 in Figure 15), indicating that cleavage mechanism of compound **1** is more efficiently under oxidative conditions. The presence of hydroxyl radical scavenger DMSO[42], and singlet oxygen scavenger NaN_3[44] do not affect the cleavage of pDNA (lane 8 *vs*. lane 6 and lane 10 *vs*. lane 6, respectively) and rule out the possible participation of the radicals in this oxidative process. EDTA partially inhibits double strand cleavage of pDNA to the L form when incubated with compound **1** and H_2O_2 (Lane 12 *vs*. Lane 6) so the compound **1** has a key role in the cleavage process. The efficiency of complex **1** cleavage is enhanced by H_2O_2, but hydroxyl radical and singlet oxygen do not appear to be involved in this process (Figure 17). These results indicate a hydrolytic mechanism of pDNA cleavage. Nevertheless, we were not able to confirm the enzymatic re-ligation of linearized DNA (with T4 DNA ligase) (Figure 18).

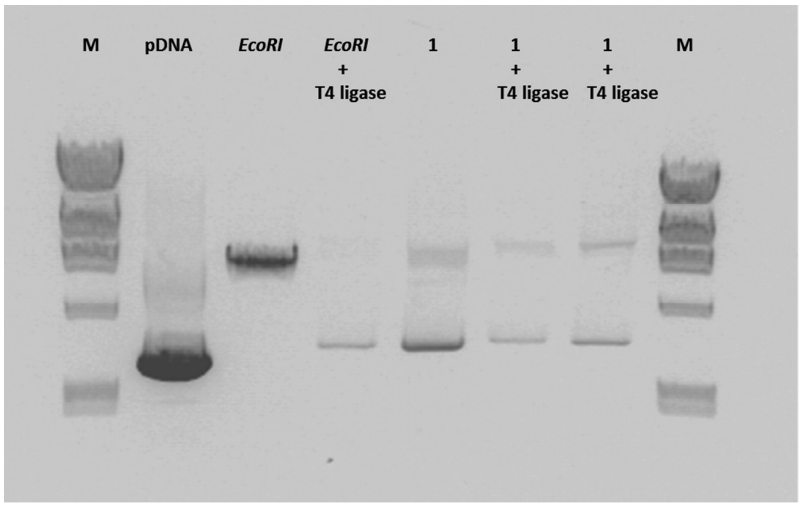

Figure 18 – T4 DNA ligase re-ligation assay. Agarose gel electrophoresis (0.7 % (w/v)) showing the double stranded cleavage of pUC18 DNA (200 ng) by compound **1** (50 μM) and the failure of T4 DNA ligase to re-ligate the fragment ends. Incubation overnight at 16 °C in T4 DNA ligase buffer was performed. Lane 1 (M): molecular marker; Lane 2 (pDNA) - pUC18; Lane 3 – linearized pUC18 using *ECORI*; Lane 4: re-ligation of blunt ends produced by pUC18 digestion with *EcoRI*; Lane 5: pUC18 incubated with compound **1** (50 μM); Lane 6 and 7 – Incubation of T4 DNA ligase with cleavage double strand pUC18 (50 μM of compound **1**).

Such a behaviour is not unprecedented in Cu(II)-based hydrolytic systems as this type of experiments might fail due to other reasons besides the presence of non-natural fragments derived from oxidative damage (*e.g.* hydrolytic fragments which do not end with the required 5'-phosphate and 3'-OH (ribose) termini)[45].

In order to evaluate the oxygen dependent or independent cleavage mechanism, pDNA cleavage under anaerobic conditions was performed (Figure 19).

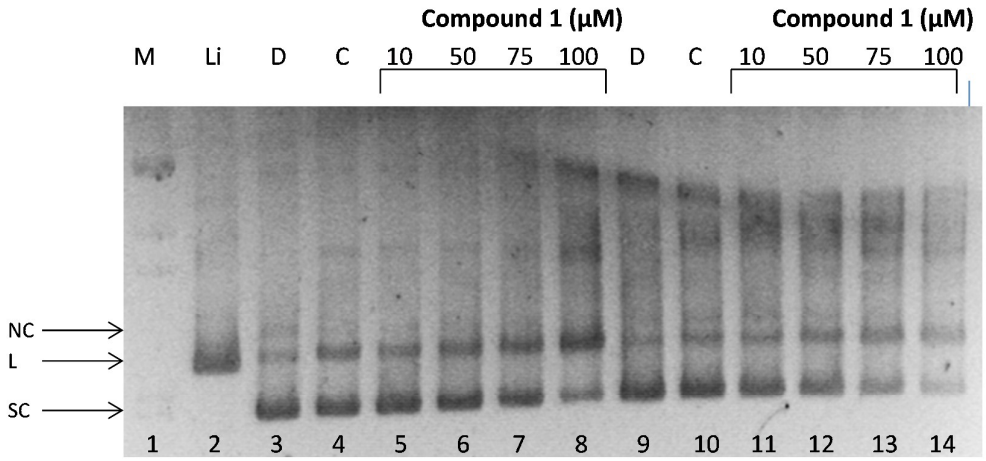

Figure 19 – DNA cleavage by compound **1**. Agarose gel electrophoresis (0.7 % (w/v)) showing the cleavage of pUC18 DNA (200 ng) by different compound **1** concentrations (10-100 μM) and DMSO (control, C). Assay was performed under anaerobic (lanes 3-8) or aerobic conditions (lanes 9-14). Incubation for 24 h at 37 °C in 5mM Tris-HCl and 50 mM NaCl buffer (pH 7.2). Lane 1 (M): molecular marker; Lane 2 (Li) - pUC18 linearized; lanes 3 and 9 (D): pUC18; lanes 4 and 10 (C): pUC18 incubated with DMSO; lanes 4-8 and 11-14: pUC18 incubated with increasing concentrations of compound **1** (10, 50, 75 and 100 μM); SC – supercoiled form; NC – nicked circular form; L – linear form.

Under anaerobic conditions, pDNA cleavage displays a similar pattern to that of aerobic conditions (Figure 19). As previously shown (Figure 14-15) the SC form shows a decrease (more evident in Figure 19 for 100 μM of **1**), which corresponds to the increase observed in the L form. The NC form also decreases with increasing concentration of DNA. The direct conversion of SC form to L occurs through double strand breaks (Figure 19). Since the assay is performed under nitrogen atmosphere, one might state that cleavage occurs through hydrolytic mechanism.

Conclusion

Five Cu(II) complexes were obtained by reaction of 4′-phenyl-terpyridine with *p*-toluenesulfonate, benzoate and monohydroxybenzoate copper salts. They present highly distorted octahedral geometries with the presence of hydroxyl groups conditioning the relative orientations of the carboxylate moieties. Relevant

intermolecular π···π contacts could be found, and the medium-strong hydrogen bond interactions led to infinite 1D chains (in **1** and **4**) and to an infinite 2D network (in **5**).

The compounds show good anti-proliferative activities against HCT116 and HepG2 tumour cells lines. The cationic compound **1** is the most cytotoxic against both tumour cells lines and the neutral compound, **4**, with *m*-hydroxylbenzoate ligands, shows the best antiproliferative activity. Additionally, compounds **1** and **4** present lower IC_{50} values for HCT116 and HepG2 tumour cells than the common antitumour drugs cisplatin and doxorubicin and all the compounds show higher antiproliferative potential in tumour cells lines compared to normal fibroblasts which is an important feature that deserves further development. The antiproliferative potential of compound **1** is due to an increase of the apoptotic process that was confirmed by Hoechst staining, flow cytometry by double staining with Anexin-FITC/PI and RT-qPCR. Indeed we observed an increase of *BAX*/*BCL-2* ratio and *CASP3* mRNA levels for 6 and 12 h compared with 1 h incubation in the presence of the compound **1**. With increasing concentration of CT-DNA, the absorption bands of the compounds are affected, resulting in the tendency of hypochromism and a minor red shift, indicating a non-covalent intercalative binding of the compounds to the DNA helix, due to the stacking interaction between the aromatic rings of the compounds and base pairs of DNA. All five compounds are able to induce *in vitro* pDNA double-strand breaks in the absence of H_2O_2 but, as demonstrated for compound **1**, the hydroxyl radical and the singlet oxygen do not appear to be involved in this process. The fact that, under anaerobic conditions, pDNA cleavage displays a similar pattern to that of aerobic conditions points out to a hydrolytic mechanism of cleavage.

This work provides good candidates for further antitumor research and deserves to be extended to other substituted terpyridine copper complexes in order to develop studies on substituent effects and to establish structure-cytotoxicity and/or structure-thermal stability relationships.

3. Experimental

3.1. Instrumentation and reagents

Elemental analyses were determined with an Elementar Vario EL III Elemental Analyser. IR spectra were measured with a Perkin–Elmer Spectrum 2000 or a Magna750 FT-IR spectrophotometer, in KBr pellets. TG-DTA data were collected with a Perkin Elmer STA6000 Simultaneous Thermal Analyzer at a heating rate of 10 K min^{-1} under an air atmosphere.

Electrospray mass spectra (ESI-MS) were run in DMSO with an ion-trap instrument (Varian 500-MS LC Ion Trap Mass Spectrometer) equipped with an electrospray ion source. For electrospray ionization, the drying gas and flow rates were optimized according to the particular sample with 35 p.s.i. nebulizer pressure. Scanning was performed from m/z 100 to 1100 in DMSO solution. The compounds were observed in the positive or negative mode (capillary voltage = 80–105 V).

Molar conductances of the complexes were determined in DMSO at room temperature by using a Jenway model 4070 conductivitymeter.

All reagents used in the experiments were of analytical grade or purified by standard methods.

3.2 Syntheses

4′-Ph-terpy (L) was prepared by following a reported procedure. [46] $Cu(OCOPh)_2$ was synthesized by the reaction of $Cu(NO_3)_2 \cdot 2.5H_2O$ with NaOCOPh in water and washed with methanol. The other copper salts were prepared by the reaction of $Cu(OH)_2$ and the respective acids. The X-ray diffraction, microanalysis and TG-DTA experiments were obtained from different batches of the respective reactions (**1** is exception).

[Cu(*p*-$SO_3C_6H_4CH_3$)L(H_2O)$_2$](*p*-$SO_3C_6H_4CH_3$) (1)

40 mL of a dichloromethane solution of L (0.46 g, 1.5 mmol) were added dropwise to 40 mL of a methanol solution of Cu(*p*-$SO_3C_6H_4CH_3)_2 \cdot$MeOH (0.50 g, 1.5 mmol) and the system was stirred for 24 h. The blue solution thus formed was concentrated and the blue solid of **1** was obtained by adding 20 mL of diethyl ether. It

was separated by filtration, washed with dichloromethane and diethyl ether and dried under vacuum (0.84 g, 75 % yield based on L). Suitable crystals for X-ray analysis were obtained upon slow evaporation of a methanol solution of **1**. Anal. calcd for $C_{28}H_{26}CuN_3O_5S \cdot C_7H_7O_3S$ (*mm* = 751.3) C 55.95, H 4.43, N 5.59. Found: C 56.09; H 4.38; N 5.41. TG-DTA determination: H_2O = 4.5 %, CuO = 12.7 %; Calc by formula $C_{35}H_{29}N_3O_6S_2Cu \cdot 2H_2O$: H_2O = 4.8 %, CuO = 10.6 %. IR (KBr disc) (cm^{-1}): 3437 (s), 3058 (s), 2917, 1613 (s, $\nu_{pyridyl\text{-}H}$), 1572 (m), 1549 (m, $\nu_{aryl\text{-}H}$), 1474 (s), 1415 (s, $\nu_{pyridyl\text{-}H}$), 1217 (s), 1192 (s), 1123 (s), 1034 (s), 1012 (s), 896 (w), 805 (m), 769 (m), 733 (w), 683 (s), 642 (m), 570 (s).
ESI-MS (m/z): 582 $[\{CuL(SO_3C_6H_4CH_3)(H_2O)_2\}+2H\}^+$; 543 $[CuL(SO_3C_6H_4CH_3)]^+$.

[Cu(OCOPh)$_2$L] (2)

$Cu(OCOPh)_2 \cdot MeOH$ (0.34 g，1.0 mmol) and L (0.31 g, 1.0 mmol) were dissolved in 30 mL methanol in a 50 mL flask and stirred for 24 h at ambient temperature. The blue solution was filtered and concentrated. The formed blue solid was washed by CH_3CN (2 × 10 mL) and **2** was obtained (0.51 g, 81 % yield based on L). Suitable crystals for X-ray analysis were obtained upon slow evaporation of a methanol solution of **2**. Anal. calcd (using another batch of the reaction, also sent for TG-DTA) for $C_{35}H_{25}CuN_3O_4 \cdot 0.6H_2O$ (*mm* = 625.5): C 67.16; H 4.22; N 6.71. Found: C 66.97; H 3.97; N 6.69. TG-DTA determination: CuO = 14.4 %; calc. by formula $C_{35}H_{25}CuN_3O_4 \cdot 0.6H_2O$: CuO = 13.0 %. IR (KBr disc) (cm^{-1}): 3061 (m), 1599 (vs, $\nu_{pyridyl\text{-}H}$), 1557 (s, $\nu_{aryl\text{-}H}$), 1475 (m, $\nu_{pyridyl\text{-}H}$), 1446 (w), 1417 (s, $\nu_{pyridyl\text{-}H}$), 1386 (vs) 1370 (s), 1305 (m), 1251 (m), 1157 (m), 1099 (w), 1068 (m), 1022 (m), 898 (w), 842 (w, $\delta_{Ar\text{-}H}$), 795 (m, $\delta_{Ar\text{-}H}$), 769 (s), 716 (s), 686 (s), 656 (w), 628 (w), 498 (w), 418 (w).
ESI-MS (m/z): 618 $[\{CuL(OCOPh)_2\}+3H]^+$; 493 $[CuL(OCOPh)]^+$.

[Cu(*o*-OCOC$_6$H$_4$OH)$_2$L] (3)

20 mL of a dichloromethane solution of L (0.31 g, 1.0 mmol) were added dropwise to 60 mL of a mixture solution of $Cu(o\text{-}OCOC_6H_4OH)_2 \cdot 2H_2O$ (0.37 g, 1.0 mmol) in methanol and DMF (2:1) in a 100 mL flask and the mixture was stirred for

24 h. Concentration and adding of diethyl ether led to the formation of a green powder of **3**, which was washed by CH_3CN (2 × 10 mL) and dried in a desiccator (0.59 g, 81 % yield based on L). Suitable crystals for X-ray analysis were obtained upon slow evaporation of the filtrate solution of **3**. Anal. calcd for $C_{35}H_{25}CuN_3O_6 \cdot 0.4CH_3CN \cdot 0.8CH_2Cl_2$ (*mm* = 731.5): C 60.09; H 3.83; N 6.51. Found: C 59.84; H 3.81; N 6.59. TG-DTA determination: CuO = 13.4 %; calc. by formula $C_{35}H_{25}CuN_3O_6$: CuO = 12.3 %. IR (KBr disc) (cm^{-1}): 3436 (s, br, ν_{OH}), 3062 (m, br, ν_{OH}), 1602 (s, $\nu_{pyridyl\text{-}H}$), 1475 (w, $\nu_{pyridyl\text{-}H}$), 1418 (m, $\nu_{pyridyl\text{-}H}$), 1387 (s), 1327 (m), 1252 (s), 1142 (m), 1067 (w), 1022 (m), 890 (m, $\delta_{Ar\text{-}H}$), 863 (m), 793 (m, $\delta_{Ar\text{-}H}$), 766 (s, $\delta_{Ar\text{-}H}$), 728 (m), 706 (m), 672 (m), 628 (m), 587 (w), 537 (w).
ESI-MS (m/z): 654 $[Cu(OCOC_6H_4OH)L(DMSO)_2]^+$; 509 $[CuL(OCOC_6H_4OH)]^+$.

[Cu(*m*-$OCOC_6H_4OH)_2$L] (4)

20 mL of a dichloromethane solution of L (0.25 g, 0.81 mmol) were added dropwise to 30 mL of a methanol solution of Cu(*m*-$OCOC_6H_4OH)_2 \cdot 0.5H_2O$ (0.28 g, 0.81 mmol) in a 100 mL flask and the mixture was stirred for 24 h. Concentration and adding diethyl ether led to the formation of a green powder of **4**, which was dried in a desiccator (0.49 g, 83 % yield based on L). Suitable crystals for X-ray analysis were obtained upon slow evaporation of a methanol solution of **4**. Anal. Calcd for $C_{35}H_{25}CuN_3O_6 \cdot CH_3OH \cdot 0.6CH_2Cl_2$ (from another reaction trial; *mm* = 730.1): C 60.21; H 4.17; N 5.76. Found: C 60.44; H 3.79; N 5.96. TG-DTA determination (from another batch of the reaction): solvent (CH_3OH) = 2.5 %, CuO = 11.9 %; calc. by formula $C_{35}H_{25}CuN_3O_6 \cdot 0.5CH_3OH$: solvent (CH_3OH) = 2.4 %, CuO = 12.0 %. IR (KBr disc) (cm^{-1}): 3435 (br, w, ν_{OH}), 3076 (w), 1613 (vs, br, $\nu_{pyridyl\text{-}H}$), 1560 (vs, br, $\nu_{phenyl\text{-}H}$), 1476 (m, $\nu_{pyridyl\text{-}H}$), 1447 (w), 1417 (w, $\nu_{pyridyl\text{-}H}$), 1375 (ws, br,), 1304 (w), 1264 (w), 1245 (s), 1161 (w), 1110 (w), 1022 (m), 1000 (w), 935 (w), 896 (m, $\delta_{Ar\text{-}H}$), 804 (m), 769 (s, $\delta_{Ar\text{-}H}$), 730 (w, $\delta_{Ar\text{-}H}$), 684 (s), 657 (w), 629 (w), 461 (w).
ESI-MS (m/z): 547 $[CuL(DMSO)_3]^+$; 509 $[CuL(OCOC_6H_4OH)]^+$.

[Cu(*p*-$OCOC_6H_4OH)_2$L] (5)

20 mL of a dichloromethane solution of L (0.15 g, 0.50 mmol) was added dropwise to 60 mL of a mixture solution of Cu(*p*-$OCOC_6H_4OH)_2 \cdot H_2O$ (0.18 g, 0.50 mmol) in methanol and DMF in a 100 mL flask and the mixture was stirred for 24 h. Filtration led to the separation of a green powder of **5** from the mother solution, which was washed by CH_3CN (2 × 10 mL) and dried in a desiccator (0.23 g, 61 % yield based on L). Suitable crystals for X-ray analysis were obtained upon slow diffusion of diethyl ether into the filtrate solution. Anal. calcd for $C_{35}H_{25}CuN_3O_6 \cdot 1.5CH_3CN \cdot 0.9CH_2Cl_2$ (using another batch of the reaction; *mm* = 785.2): C 59.51; H 4.02; N 8.03. Found: C 59.32; H 4.16; N 8.12. TG-DTA determination (using another batch of the reaction): solvent (CH_3CN) = 7.5 %, CuO = 12.4 %; calc. by formula $C_{35}H_{25}CuN_3O_6 \cdot 1.3CH_3CN$: solvent ($CH_3CN$) = 7.6 %, CuO = 11.4 %. IR (KBr disc) (cm^{-1}): 3467 (vs, br, ν_{OH}), 2427 (-CN), 1612 (vs, br, $\nu_{pyridyl\text{-}H}$), 1552 (s, $\nu_{aryl\text{-}H}$), 1474 (m, $\nu_{pyridyl\text{-}H}$), 1441 (w, $\nu_{pyridyl\text{-}H}$), 1384 (vs), 1283 (s), 1245 (s), 1168 (m), 1098 (w), 1020 (m), 892 (w), 846 (w, $\delta_{Ar\text{-}H}$), 796 (m, $\delta_{Ar\text{-}H}$), 769 (m, $\delta_{Ar\text{-}H}$), 695 (w), 619 (w).

ESI-MS (m/z): 725 $[\{Cu(OCOC_6H_4OH)_2L(DMSO)\}+2H]^+$; 654 $[Cu(OCOC_6H_4OH)L(DMSO)_2]^+$; 509 $[Cu(OCOC_6H_4OH)L]^+$.

3.3. Crystal structure determinations

X-ray quality single crystals of the compounds were mounted in a nylon loop and measured 150 K (**4** and **5**) or at room temperature (**1** – **3**). Intensity data were collected using a Bruker AXS-KAPPA APEX II diffractometer with graphite monochromated Mo-Ká (ë 0.71069) radiation. Data were collected using phi and omega scans of 0.5° per frame and a full sphere of data was obtained. Cell parameters were retrieved using Bruker SMART[47] software and refined using Bruker SAINT[47] on all the observed reflections. Absorption corrections were applied using SADABS[47]. Structures were solved by direct methods by using the SHELXS package[48a] and refined with SHELXL-2014[48b]. Calculations were performed using the WinGX System–Version 1.80.03[49]. The hydrogen atoms of hydroxyl groups (in **3** – **5**) and those of

coordinated water molecules (in **1**) were found in the difference Fourier map and the isotropic thermal parameters were set at 1.5 times the average thermal parameters of the belonging oxygen atoms. Coordinates of hydrogen atoms bonded to carbon atoms were included in the refinement using the riding-model approximation with the Uiso(H) defined as 1.2Ueq of the parent aromatic atoms and as 1.5Ueq of the parent carbon atoms for the methyl groups. There were disordered molecules present in the structure of **5**. Since no obvious major site occupations were found for those molecules, it was not possible to model them. PLATON/SQUEEZE[50] was used to correct the data and a potential volume of 605.8 $Å^3$ was found with 159 electrons per unit cell worth of scattering. The refinement with (without) the model treatment gives R1 values of 0.0368 (0.0915) thus improving this parameter by 60%. The disordered molecules could not be identified. Moreover, the phenyl moiety in **5** is disordered over two orientations and were refined with the use of PART instruction and refined to a ratio of 68% and 32%. Least square refinements with anisotropic thermal motion parameters for all the non-hydrogen atoms and isotropic ones for the remaining atoms were employed. Crystallographic data are summarized in Table 6. CCDC 941486, 941487, 941488, 941489 and 941490 contain the supplementary crystallographic data for this paper. These data can be obtained free of charge from the Cambridge Crystallographic Data Centre via w.ccdc.cam.ac.uk/data_request/cif.

Table 6 – Relevant crystal data for complexes **1** – **5**.

Compounds	**1**	**2**	**3**	**4**·CH_4O	**5**
Formula	$C_{35}H_{33}CuN_3O_8S_2$	$C_{35}H_{25}CuN_3O_4$	$C_{35}H_{25}CuN_3O_6$	$C_{36}H_{29}CuN_3O_7$	$C_{35}H_{25}CuN_3O_6$
Formula Weight	751.07	614.93	64693	678.94	646.93
Crystal system	Monoclinic	Triclinic	Triclinic	Triclinic	Monoclinic
Space group	*P*2(1)/*c*	*P*-1	*P*-1	*P*-1	*P*2(1)/*c*
a(Å)	8.2850(4)	9.5993(6)	9.5127(5)	9.0848(3)	17.8398(14)
b (Å)	31.1469(17)	10.8157(7)	10.7981(6)	12.0013(4)	9.0056(7)
c (Å)	13.8987(7)	14.9401(9)	15.2472(9)	15.5065(5)	27.0152(17)
α (°)	90	95.613(3)	97.794(3)	94.097(2)	90
β (°)	112.888(3)	90.814(4)	90.711(4)	104.306(3)	128.221(4)
γ (°)	90	114.820(3)	113.681(3)	107.188(2)	90
V (Å^3)	3304.2(3)	1398.48(15)	1417.18(14)	1545.90(9)	3409.8(5)
Z	4	2	2	2	4
D_{calc} (Mg m^{-3})	1.510	1.460	1.516	1.459	1.260
μ (mm^{-1})	0.846	0.828	0.826	0.763	0.686
F(000)	1556	634	666	702	1332
θ_{max}, θ_{min} (°)	28.284, 2.526	30.160, 2.342	28.357, 2.084	28.298, 3.038	29.600, 2.457
Index range *h*	-11→10	-13→11	-12→12	-9→12	-24→24
K	-40→41	-15→12	-14→14	-15→15	-12→12
L	-18→18	-21→20	-20→20	-20→20	-37→37
Independent reflections	8145	7815	7037	7458	9495
Observed reflections	6516	6069	6230	6215	6772
R_{int}	0.0348	0.0253	0.0167	0.0211	0.0240
R	0.0377	0.0409	0.0384	0.0326	0.0368
w*R*	0.0886	0.1041	0.1148	0.0766	0.0986
GOF	1.041	1.052	1.014	1.030	1.015

3.4 Assessment of the cytotoxicity of the copper compounds

Cell culture. Two tumour cell lines from human colorectal carcinoma (HCT116) and human hepatocellular carcinoma (HepG2) were grown as reported[44]. Normal human fibroblasts were grown in the same conditions as HepG2 cell line and were kindly provided by Carreira I. (Laboratory of Cytogenetics and Genomics, Faculty of Medicine, University of Coimbra, Portugal).

Compound exposure. For the dose–response curves, cells were plated at 7500 cells per well in 96-well plates. Consumed media was removed 24 h after platting and

replaced with fresh media containing: 0.01, 0.025, 0.05, 0.1, 0.5, 1, 5 and 10 μM of compound **1** - **5**; or 0.1% (v/v) DMSO (vehicle control). All previous solutions were prepared from 1000-times concentrated stock solutions of the compounds to assure a maximum volume of DMSO in culture medium of 0.1 % (v/v).

Viability assays. After 48 h of cell incubation in the presence of each compound and vehicle control, cell viability was evaluated using CellTiter 96® AQueous Non-Radioactive Cell Proliferation Assay (Promega, Madison, WI, USA), as described in[51]. All data were expressed as mean ± SEM from at least three independent experiments.

Hoechst 33258 labelling. HCT116 and HepG2 cells were plated in 35 mm dishes at $2x10^5$ cells/dish. Culture medium was removed 24 h after platting and replaced with 2 mL of fresh medium containing 0.05 and 0.1 μM of compound **1** or DMSO (0.1% (v/v)). Cells were stained with Hoechst 33258 after an incubation period of 24 h as described elsewhere[44].

Annexin V-FITC/PI double-staining assay. HCT116 cells were seeded into 25 cm^2 culture flasks at $2.25x10^5$cells/flask. Culture medium was removed 24 h after platting and replaced with 3 mL of fresh medium containing either 0.05 or 0.1 μM of compound **1** or DMSO (0.1 % (v/v)). Cells were incubated for 48 h and then stained with propidium iodide (PI) and fluorescein isothiocyanate (FITC) labelled Annexin V according to the manufacturer's instructions (Annexin V-FITC Apoptosis Detection Kit; Invitrogen, Carlsbad, CA, USA) as previously described[51;52]. Data was collected on Attune® Acoustic Focusing Flow Cytometer (Life Technologies, Carlsbad, California) and analyzed with Attune® Cytometric software (Life Technologies).

Apoptotic gene expression by RT-qPCR. HCT116 cells were seeded into 25 cm^2 culture flasks at $2x10^5$cells/flask. Culture medium was removed 24 h after platting and replaced with 3 mL of fresh medium containing either 0.1 μM of compound **1** or

DMSO. Cells were incubated for 1, 6 and 12 h. Cells were collected, washed with 1x cold phosphate-buffered saline (PBS). Total RNA was extracted from the cell pellet using the SV Total RNA Isolation System Kit (Promega) and cDNA was synthesized using cDNA Synthesis Kit (Bioline, London, UK), both according to the manufacturers' instructions. Real-time PCR amplification was performed in a LightCycler® 480 (Roche, Basel, Switzerland) using SensiFASTTM SYBR No-ROX Kit (Bioline) in 10 µL reactions containing 5 µL of 2x SensiFAST SYBR No-ROX Mix, 85 ng of cDNA and 0.30 pmol/µL of each primer. Forward and reverse primer sequences and specific annealing temperatures are shown in Table 7.

Table 7 – Primers and annealing temperatures used for RT-qPCR.

Gene	Encoded protein	Forward primer (5'–3')	Reverse primer (5'–3')	$T_{annealing}$ (°C)	Product size (bp)	Reference
rRNA18S5	Ribossomal major subunit	GTAACCCGTTGAACCCCATT	CCATCCAATCGGTAGTAGCG	59	151	[53]
BAX	BAX	TGCTTCAGGGTTTCATCCAGGA	ACGGCGGCAATCATCCTCTG	62	172	[54]
BCL-2	BCL-2	CTTCGCCGAGATGTCCAGCCA	CGCTCTCCACACACATGACCC	65	152	
CASP3	Caspase 3	TACCAGTGGAGGCCGACTTC	GCACAAAGCGACTGGATGAAC	59	103	

The amplification conditions consisted of 95 °C for 2 min, followed by 40 cycles of (i) denaturation at 95 °C for 5 sec, annealing at 59-65 °C for 10 sec and (iii) extension at 72 °C for 10 sec. All the results were originated from three independent experiments. Threshold cycle values were analyzed by the $2^{-\Delta\Delta Ct}$ method[55]. The *rRNA18S5* expression levels were used as reference to normalize the expression of the apoptotic genes. The results were expressed as the ratio of reference gene to target gene by using the following equation (1):

$$\Delta Ct = Ct \text{ (target gene)} - Ct \text{ (control gene)} \quad (1)$$

The relative expression levels were determined using the equation (2):

$\Delta\Delta Ct = \Delta Ct$ (treated sample) – ΔCt (control) (2)

The expression of apoptotic genes was calculated using the expression of $2^{-\Delta\Delta Ct}$. The PCR products were subjected to electrophoresis on a 2 % (w/v) agarose gel (TAE 1x) during 50 min at 5 V/cm, stained with GelRed (Biotarget, Portugal) and photographed using a UVI TEC transilluminator (Cambridge, UK) coupled to a Kodak AlphaDigiDoc camera (Alpha Innotech, California, USA). Image acquisition was performed using AlphaEaseFC software (AlphaDigiDoc 1000, Alpha Innotech).

Absorption spectroscopy Interaction of compounds **1-5** with Calf Thymus DNA (CT-DNA; Invitrogen) was assessed by UV-Visible spectroscopy (230 to 400 nm) in an Evolution 300 UV-Vis spectrophotometer (Thermo Scientific). CT-DNA concentration per nucleotide was previously determined at 260 nm in a NanoDrop2000 (Thermo Scientific) using an extinction coefficient of 6600 $M^{-1}cm^{-1}$. UV spectra were acquired using 15 µM of each compound and in absence or presence of CT-DNA (concentration between 0-30 µM). All solutions were prepared in Tris-HCl 5 mM, NaCl 50 mM buffer (pH 7.2) and incubated at 37 °C for 24 h. Binding constants, K_b, were determined using the equation (3):

$$\frac{[DNA]}{(\varepsilon_a-\varepsilon_f)} = \frac{[DNA]}{(\varepsilon_b-\varepsilon_f)} + \frac{1}{K_b(\varepsilon_b-\varepsilon_f)} \quad (3)$$

where ε_a, ε_f and ε_b are the apparent extinction coefficient, the extinction coefficient for the free compound and the extinction coefficient for the compound in the fully bound form, respectively [Aslanoglu M (2006) Anal Sci 22:439-443]. ε_a correspond to Aobs/[compound] and ε_f were determined through calibration curves of each metal compound in Tris-HCl 5 mM, NaCl 50 mM buffer (pH 7.2)[56]. From the graphical

analysis of [DNA]/(ε_a-ε_f) versus [DNA], it is known that (1/(ε_b-ε_f)) corresponds to the slope and Y intercept equal to (1/Kb(ε_b-ε_f)). K_b corresponds to the ratio between slope and the Y intercept[56].

Interaction between compounds 1-5 and plasmid DNA. pBluescript II SK(+) (pBSK II) DNA and plasmid DNA pUC18 (Thermo Scientific) were obtained from *E.coli* transformed cells, grown overnight in Luria-Bertani liquid medium (LB; Applichem, Darmstadt, Germany) with 100 μg/mL Ampicillin (Bioline, London, UK), at 37 °C, gently stirring. Plasmid extractions were performed using the NZYMiniprep (Nzytech, Portugal), according to the manufacturer's instructions, except for the elution step in which was used 50 mM Tris-HCl, 10 mM NaCl (pH 7.25), preheated at 70 °C. DNA was quantified by spectrophotometry with NanoDrop2000.

Interaction between compounds **1-5** and pDNA was performed with 200 ng of pBSK II and compounds **1-5** at different concentrations (5-100 μM) in 5 mM Tris-HCl, 50 mM NaCl buffer (pH 7.2). Control sample consisted of pBSK II and buffer with or without 3 % (v/v) of DMSO. Samples were incubated at 37 °C for 24 h.
Similarly, to assess the kinetics of the reaction, 200 ng of pBSK II with either 10 or 50 μM of compound **1** in 5 mM Tris-HCl, 50 mM NaCl (pH 7.2) were incubated at 37 °C for 1, 5, 20, 24 and 48 h.

In vitro interaction between compound **1** and pDNA was performed under anaerobic conditions by incubating pUC18 (200 ng) and compound **1** at different concentrations (10, 50, 75 and 100 μM) with and without 3 % (v/v) DMSO in 5 mM Tris-HCl, 50 mM NaCl buffer (pH 7.2). Samples were placed in a desiccator and three cycles of vacuum-nitrogen atmosphere were performed. The vials were sealed under nitrogen atmosphere, and incubated at 37 °C for 24 h.

Compound-pDNA interaction assays were performed in tubes containing 200 ng of pUC18 and 50 μM compound **1** in the presence or absence of the activating agent H_2O_2 (2 mM) in 5 mM Tris- HCl, 50 mM NaCl (pH 7.2) (reaction volume 20 μL). The control sample was prepared with 3 % (v/v) DMSO and all samples were incubated at 37 °C for 24 h with or without H_2O_2 or reductive agents. After the incubation, samples were treated as previously described[44].

To further characterize the pDNA cleavage mechanism (namely through hydrolysis), the re-ligation capability of T4 DNA ligase (New England Biolabs, UK) towards double cleaved pUC18 pDNA (incubation of pUC18 (200 ng) in the presence of compound 1 (50 μM) or in the presence of *EcoRI* for 24 h at 37 ºC was assessed. Briefly a mixture of double cleaved pUC18 DNA, T4 DNA ligase buffer and the enzyme were gently mixed (Table 8) and incubated overnight at 16°C (for both cohesive (sticky) ends and blunt ends). Samples were heat inactivate at 65°C for 10 minutes.

Table 8 – T4 DNA Ligase assay mixture

Reagent	20 μl REACTION
10X T4 DNA Ligase Buffer	2 μl
pUC18 DNA	200 ng
Nuclease-free water	to 20 μl
T4 DNA Ligase	1 μl

Stability of compounds 1-5 in biological conditions. In order to assess compounds stability in biological conditions phosphate buffered saline (PBS) (pH 7.0) was used. Compounds (20 μM) were incubated in PBS for 1, 3, 6, 12 and 24 h at 37 ºC and UV spectra were acquired (240 to 440 nm) in an Evolution 300 UV-Vis spectrophotometer (Thermo Scientific).

Acknowledgements

The authors are grateful for the financial support from the Foundation for Science and Technology (FCT), Portugal, and its programs (POCI, FEDER funded, Grant No. SFRH/BPD/24691/2005, PTDC/BBB-NAN/1812/2012, UID/QUI/00100/2013 and UID/Multi/04378/2013 project), the Science Foundation of China (21261002). The authors thank Ana Silva for preliminary technical support of the viability data of compounds **1-5** and Lidia Coito and Fabiana Paradinha for technical support concerning biological data of compounds **1-5**.

References

1 (a) R. Trokowski, S. Akine and T. Nabeshima, *Chem. Commun.*, 2008, 889-890; (b) Y. Hasegawa, T. Nakagawa and T. Kawai, *Coord. Chem. Rev.*, 2010, **254**, 2643-2651; (c) V. W.-W. Yam and K. K.-W. Lo, *Chem. Soc. Rev.*, 1999, **28**, 323-334.

2 (a)V. W.-W. Yam, C.-K. Hui, S.-Y. Yu and N. Zhu, *Inorg. Chem*., 2004, **43**, 812-821; (b) L. Hou and D. Li, *Inorg. Chem. Commun*., 2005, **8**, 128-130; (c) Z. Ma, B. Liu, H. Yang, Y. Xing, M. Hu and J. Sun, *J. Coord. Chem.*, 2009, **62**, 3314-3323.

3 (a) Effendy, F. Marchetti, C. Pettinari, B.W. Skelton and A.H. White, *Inorg. Chim. Acta*, 2007, **360,** 1433-1450; (b) J.D. Crowley, A.J. Goshe, I.M. Steele and B. Bosnich, *Chem.-Eur. J.*, 2004, **10**, 1944-1955; (c) A. Hussain, S. Gadadhar, T.K. Goswami, A.A. Karande and A.R. Chakravarty, *Eur. J. Med. Chem.*, 2012, **50**, 319-331.

4 (a) J. Muller, E. Freisinger, P. Lax, D.A. Megger and F.-A. Polonius, *Inorg. Chim. Acta*, 2007, **360**, 255-263; (b) J.S. Field, C.R. Wilson and O.Q. Munro, *Inorg. Chim. Acta*, 2011, **374**, 197-204; (c) N.W. Alcock, P.R. Barker, J.M. Haider, M.J. Hannon, C.L. Painting, Z. Pikramenou, E.A. Plummer, K. Rissanen and P. Saarenketo, *J. Chem. Soc., Dalton Trans*., 2000, 1447-1449.

5 (a) S.-S. Zhang, S.-Z. Zhan, M. Li, R. Peng and D. Li, *Inorg.Chem*., 2007, **46,**

4365-4367; (b) M. Liu, Z. Ye, G. Wang and J. Yuan, *Talanta*, 2012, **91**, 116-121; (c) T. Yutaka, I. Mori, M. Kurihara, J. Mizutani, N. Tamai, T. Kawai, M. Irie and H. Nishihara, *Inorg. Chem*., 2002, **41**, 7143-7150.

6 (a) M. Barboiu, L.Prodi, M. Montalti, N. Zaccheroni, N. Kyritsakas and J.-M. Lehn, *Chem. -Eur. J.*, 2004, **10,** 2953-2962; (b) R. Dobrawa and F. Würthner, *Chem. Commun.*, 2002, 1878-1879.

7 (a) J.S. Field, R. J. Haines, L.P. Ledwaba, R. McGuire Junior, O.Q. Munro, M.R. Low and D.R. McMillin, *Dalton Trans.*, 2007, 192-199; (b) P. Song, S. Sun, S. Wang, F. Ma, Y. Xu and X. Peng, *Spectrochim. Acta A: Mol. Biomol. Spectrosc.*, 2011, **81**, 283-289.

8 (a) E. Shikhova, E.O. Danilov, S. Kinayyigit, I.E. Pomestchenko, A.D. Trebulov, F. Camerel, P. Retailleau, R. Ziessel and F.N. Castellano, *Inorg. Chem*., 2007, **46**, 3038-3048; (b) H. Padhy, D. Sahu , I-H. Chiang , D. Patra , D. Kekuda , C.-W. Chu and H.-C. Lin, *J. Mater. Chem.*, 2011, **21**, 1196-1205.

9 Y. Fan, Y.-M. Zhu, F.-R. Dai, L.-Y. Zhang and Z.-N. Chen, *Dalton Trans.,* 2007, 3885-3892.

10 P. Du, J. Schneider, W.W. Brennessel and R. Eisenberg, *Inorg. Chem.*, 2008, **47**, 69-77.

11 C. Hamann, J.-M. Kern and J.-P. Sauvage, *Dalton Trans.*, 2003, 3770-3775.

12 (a) Z. Ma, Y. Xing, M. Yang, M. Hu, B. Liu, M.F.C. Guedes da Silva and A.J.L. Pombeiro, *Inorg. Chim. Acta*, 2009, **362**, 2921-2926; (b) Z. Ma, W. Lu, B. Liang and A.J.L. Pombeiro, *New J. Chem.,* **2013**, 37, 1529-1537; (c) Z. Ma, L. Wei, E.C.B.A. Alegria, L.M.D.R.S. Martins, M.F.C. Guedes da Silva and A.J.L. Pombeiro, *Dalton Trans*., 2014, **43**, 4048-4058.

13 K.W. Jennette, S.J. Lippard, G.A. Vassiliades and W.R. Bauer, *Proc. Natl. Acad. Sci. USA*, 1974, **71**, 3839-3843.

14 L.X. Zhao, J. Sherchan, J.K. Park, Y. Jahng, B.S. Jeong, T.C. Jeong, C.S. Lee and E.S. Lee. *Arch. Pharm. Res*., 2006 , **29**, 1091-1095.

15 M.J. MacLachlan, M. Ginzburg, N. Coombs, T.W. Coyle, N.P. Raju, J.E. Greedan, G.A. Ozin and I. Manners, *Science*, 2000, **287**, 1460-1463.

16 A. Anthonysamy, S. Balasubramanian, V. Shanmugaiah and N. Mathivanan, *Dalton Trans.* 2008, **28,** 2136-2143.

17 L.X. Zhao, T.S. Kim, S.H. Ahn, T.H. Kim, E.K. Kim, W.J. Cho, H. Choi and C.S. Lee. *Bioorg. Med. Chem. Lett.*, 2001, **11,** 2659-2664.

18 C. Marzano, M. Pellei, F. Tisato and C. Santini, *Med. Chem.*, 2009 , **9**, 185-211.

19 (a) I. Ott and R. Gust, *Arch. Pharm.*, 2007, **340,** 117-126. (b) G. Jaouen (Ed.), "Bioorganometallics: Biomolecules, Labeling, Medicine", Wiley-VCH, 2005. (c) P. Martins, M. Marques, L. Coito, A.J.L. Pombeiro, P.V. Baptista and A.R. Fernandes, *Anti-cancer Agent Med. Chem.,* 2014, **14**, 1199-1212. (d) M. Frezza, S. Hindo, D. Chen, A. Davenport, S. Schmitt, D. Tomco and Q.P. Dou. *Curr. Pharm. Des.*, 2010, **16**, 1813-1825. (e) S.M. Schmitt, M. Frezza and Q.P. Dou. *Front. Biosci. (Schol Ed).* 2012, **4**, 375-391. (f) A. Bonetti, R. Leone, F. Muggia and S.B. Howell (Ed.), "Platinum and Other Heavy Metal Compounds in Cancer Chemotherapy: Molecular Mechanisms and Clinical applications", Humana Press, 2009.

20 S. Roy, S. Saha, R. Majumdar, R.R. Dighe and A.R. Chakravarty, *Polyhedron* 2010, **29**, 2787-2794.

21 A. Kumar, J.P. Chinta, A.K. Ajay, M.K. Bhat and C.P. Rao, *Dalton Trans.* 2011, **40,** 10865-10872.

22 (a) K. Robinson, G.V. Gibbs and P.H. Ribbe, *Science* 1971, **172**, 567-570. (b) C. Janiak, *J. Chem. Soc*., *Dalton Trans*., **2000**, 3885-3896.

23 (a) Z. Ma, Y. Cao, Q. Li, M.F.C. Guedes da Silva, J.J.R. Fraústo da Silva and A.J.L. Pombeiro, *J. Inorg. Biochem.*, 2010, **104**,704-711. (b) C. Hamann, J.-M.Kern and J.-P. Sauvage, *Inorg. Chem.*, 2003, **42**, 1877-1883.

24 (a) T.T. Al-Nahary, *J. Saudi Chem. Soc.*, 2009, **13**, 253-257. (b) R.K. Boggess, J.W. Hughes, W.M. Coleman, L.T. Taylor, *Inorg. Chim. Acta* 1980, **38**, 183-189.

24 C-W. Yu, K.K.W. Li, S-K. Pang, S.C.F. Au-Yeung and Y-P. Ho, *Bio. Med. Chem. Let.,* 2006, **16**, 1686-1691.

25 L.T. Vassilev, B.T. Vu, B. Graves, D. Carvajal, F. Podlaski, Z. Filipovic, N. Kong, U. Kammlott, C. Lukacs, C. Klein, N.A. Fotouhi and E.A. Liu, *Science,* 2004, **303**,

844-848.

26. M. Porchia, A. Dolmella, V. Gandin, C. Marzano, M. Pellei, V. Peruzzo, F. Refosco, C. Santini and F. Tisato, *Eur. J. Med. Chem.*, 2013, **59**, 218–226.

27 P. Cao, X. Cai, W. Lu, F. Zhou and J. Huo, *Evid.-Based Compl. Alt.*, 2011, ID 958243, 9 pages.

27 O. Kepp, L. Galluzzi, M. Lipinski, J. Yuan and G. Kroemer, *Nat. Rev. Drug Discov.*, 2011¸ **10**, 221-237.

29 Y. Yuan, J.C. Bian, X.Z. Liu, Y. Zhang, Y. Sun and Z.P. Liu, *Biomed. Environ. Sci.*, 2012, **25**, 172-181.

30 G. Brumatti, C. Sheridan and S.J. Martin, *Methods*, 2008, **44**, 235-240.

31 C.M. Carvalho, P.F. Menezes, G.C. Letenski, C.E. Praes, I.H. Feferman and M. Lorencini, *Int. J. Cosmet. Sci*., 2012, **34**, 176-182.

32 T.F. Ho, C.J. Ma, C.H. Lu, Y.T. Tsai, Y.H. Wei, J.S. Chang, J.K. Lai, P.J. Cheuh, C.T. Yeh, P.C. Tang, J.T. Chang, J.L. Ko, T.S. Liu, H.E. Yen, and C.C. Chang, *Toxicol. Appl. Pharm.*, 2007, **225**, 318-328.

33 C. Riccardi, and I. Nicoletti, *Nat. Protoc*., 2006, **1**, 1458-1461.

34 S. Elmore, *Toxicol. Pathol*., 2007, **35**, 495-516.

35 I.M. Ghobrial, T.E. Witzig, and A.A. Adjei, *CA-Cancer J. Clin*. 2005, 55, 178-194.

36. Q.L. Zhang, J.G. Liu, H. Chao, G.Q. Xue, L.N. Ji, *J. Inorg. Biochem*. 2001, **83**, 49–55.

37. A. Oleksi, A.G. Blanco, R. Boer, J. Usón, J. Aymamí, A. Rodger, M.J. Hannon, M. Coll, *Angew. Chem. Int. Ed* 2006, **45**, 1227–1231.

38. S. Shi, J. Liu, J. Li, K. C. Zheng, X. M., Huang, C. P. Tan, L. M. Chen, and J. Ln, *Inorganic Biochemistry* 2006, **100**, 385–395

39. J.K. Barton, A.T. Danishefsky, J.M. Goldberg *J Am Chem Soc*. 1984, **106**, 2172–2176

40. H.L. Lu, J.J. Liang, Z.Z. Zeng, P.X. Xi, X.H. Liu, F.J. Chen, Z.H Xu. *Trans Metal Chem*. 2007, **32**, 564 – 569.

41. Q. Li, P. Yang, H. Wang, M. Guo. *J Inorg Biochem*. 1996, **64**, 181-95.

42 D- Li, J. Tian, Y. Kou, F. Huang, G. Chen, W. Gu, X. Liu, D. Liao, P Cheng and S. Yan, *Dalton Trans.*, 2009, 3574-3583.

43 M. Li, T. Lan, X. Cao, H. Yang, Y. Shi, C. Yi and G. Chen, *Dalton Trans*., 2014, **43**, 2789-2798.

44 T.F.S. Silva, L.M.D.R.S. Martins, M.F.C. Guedes da Silva, A.R. Fernandes, A. Silva, P.M. Borralho, S. Santos, C.M.P. Rodrigues and A.J.L. Pombeiro, *Dalton Trans.*, 2012, **41**, 12888-12897.

45 M. Scarpellini, A. Neves, R. Hörner, A.J. Bortoluzzi, B. Szpoganics, C. Zucco, R.A. Nome Silva, V. Drago, A.S. Mangrich, W.A. Ortiz, W.A. Passos, M.C. de Oliveira and H. Terenzi, *Inorg. Chem.*, 2003, **42**, 8353-8365.

46 E.C. Constable, J. Lewis, M.C. Liptrot and P.R. Raithby, *Inorg. Chim. Acta*, 1990, **178**, 47.

47 Bruker, APEX2 & SAINT. Bruker, AXS Inc., Madison, Wisconsin, USA, 2004.

48 (a) G. M. Sheldrick, *Acta Crystallogr. A*, 1990, **46**, 467. (b) G. M. Sheldrick, *Acta Crystallogr. A*, 2008, **A64**, 112.

49 L.J. Farrugia, *J. Appl. Crystallogr.*, 1999, **32**, 837-838.

50 A.L. Spek, *Acta Crystallogr. A*, 1990, **46**, C34.

51 A. Silva, D. Luís, S. Santos, J. Silva, A.S. Mendo, L. Coito, T.F.S. Silva, M.F.C. Guedes da Silva, L.M.D.R.S. Martins, A.J.L. Pombeiro, P. Borralho, M.C.M. Rodrigues, M.G. Cabral, P. A. Videira, C. Monteiro and A.R. Fernandes, *Drug Metab. Drug. Interact.* 2013, **28**, 167-176.

52 T.F.S. Silva, P. Smoleński, L.M.D.R.S. Martins, M.F.C. Guedes da Silva, A.R. Fernandes, D. Luis, A. Silva, S. Santos, P.M. Borralho, C.M.P. Rodrigues and A.J.L. Pombeiro, *Eur. J. Inorg. Chem*. 2013, 3651-3658.

53 D.V. Luís, J. Silva, A.I. Tomaz, R.F.M. de Almeida, M. Larguinho, P.V. Baptista, L.M.D.R.S. Martins, T.F.S. Silva, P.M. Borralho, C.M.P. Rodrigues, A.S. Rodrigues, A.J.L. Pombeiro and A.R. Fernandes, *J. Biol. Inorg. Chem.*, 2014, **19**, 787-803.

54 Y. Li, J. Liu and Q. Li, *Mol. Carcinog.*, 2010, **49**, 566-581.

55 K.J. Livak and T.D. Schmittgen, *Methods*, 2001, **25**, 402-408.

56. N. Shahabadi, S. Mohammadi and R. Alizadeh. *Bioinorg Chem Appl*, 2011, 1-8.

Graphical abstract

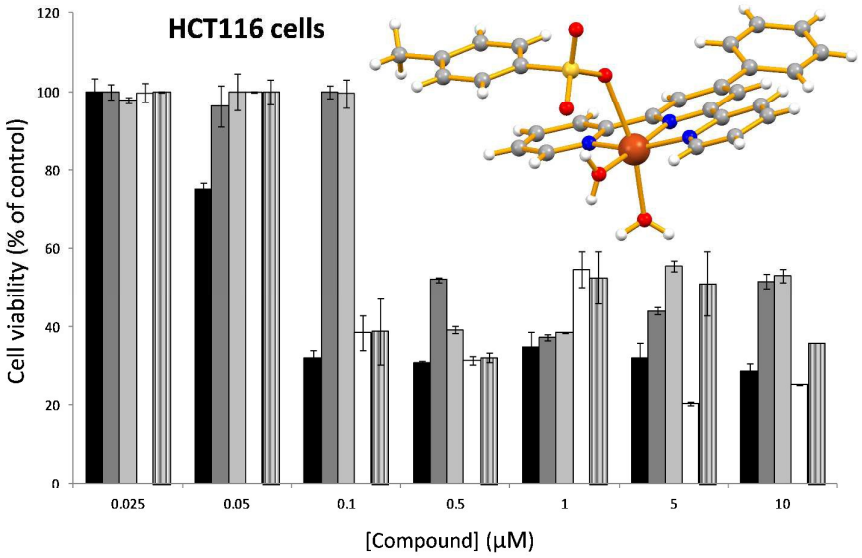

Mononuclear 4,4′-phenyl-terpyridine copper(II) complexes with *p*-toluenesulfonate, benzoate, *o*-, *m*- and *p*-hydroxybenzoate were synthesized and their cytotoxic properties studied.